ADVANCED ELECTRONIC MATERIALS
www.advelectronicmat.de

Strain Sensing by Electrical Capacitive Variation: From Stretchable Materials to Electronic Interfaces

Hussein Nesser and Gilles Lubineau**

Sensing the motion of objects and humans is essential for various applications, including human-machine interfaces. Over the past few years, motion sensing has been extensively studied using capacitive strain sensors that can be utilized for wireless communications. The performance and functionality of capacitive strain sensors have been improved by achieving high sensitivity, large-area sensing, ultra-stretchability, and simplicity in design, measurement methods, and wireless integration. This review article highlights recent developments in capacitive strain sensors, including their characteristics and applications. First, the mechanisms and techniques employed to enhance the sensitivity of capacitive strain sensors are reviewed. Then, the notable features of this sensing strategy are highlighted, such as its ability to cover a wide area, properties of the required electronic interface, and sensor implementation inside a remote measurement system via an oscillating circuit. Therefore, a global review of the capacitive strain sensor that has been previously attempted can participate in developing an effective sensing method to meet the market need.

1. Introduction

The collection of mechanical information, such as stretching, bending, pressure, and impact, is necessary for various applications. In the last decade, several methods based on optical, chemical, and electrical phenomena have been developed to detect mechanical effects from the environment. Fiber Bragg grating (FBG),[1–4] liquid metals,[5,6] Raman shift,[7,8] and piezoelectricity[9,10] have been used for strain sensing. The integration of these types of strain sensing in some applications remains challenging owing to their sophisticated measurement equipment, low flexibility, and poor resolution and performance.[11–14] Thus, this research has been oriented toward systems that respond to mechanical strain by changing their electrical properties.

Recently, stretchable and wearable strain sensors have been investigated owing to their potential applications in structural health monitoring,[15–18] personalized healthcare,[19–22] smart clothing,[23–25] human motion detection and sports performance monitoring,[26–30] soft robotics with advanced sensing capabilities,[31–34] and human–machine interfaces.[35,36] Several factors, such as material type, biocompatibility, low cost, ease of implementation, simplicity of fabrication, wireless connection capability, dimension, and power consumption, were considered in the evaluation of the strain sensors. In addition, their sensing performance was characterized based on the sensitivity or gauge factor (GF), stretchability, hysteresis, linearity, durability, overshoot behavior, response, and recovery time. In particular, stretchable strain sensors based on electrical signal variation require a simple electronic read-out system, making them suitable for various applications.

Electrical signal variation is often created by changing the conductivity of the material under deformation. Piezoresistive strain sensors made of a compliant flexible polymer or rubber charged by conductive nanomaterials have been developed. The conductive filler may comprise carbon nanotubes (CNT),[37–40] carbon grease,[41] graphene[42–44] nanowires,[45–47] nanoparticles,[48] conductive fabric,[49] ionic liquid,[50] or conductive acrylic elastomer.[51] However, the sensitivity of piezoresistive strain sensors needs to be further improved. To increase the GF of resistive strain sensors, various mechanisms have been employed, such as the tunneling effect,[48,52,53] crack generation in thin films,[37,54,55] and disconnection between sensing elements.[43]

Moreover, another electrical property influenced by strain is capacitance. In this study, the mechanisms of capacitance variation are presented in detail. Numerous studies have been conducted to compare the performances of resistive and capacitive strain sensors.[56–58] In particular, capacitive sensors provide high linearity,[59] small hysteresis,[60] and fast response time,[61] making them suitable for applications where sensors undergo repeated dynamic strains.

In this review article, recent developments in capacitive strain sensors are evaluated, including operation mechanisms, fabrication processes, and materials used for generating capacitance variation under very high or low strain. Importantly, capacitive strain sensors can cover a large area by creating a sensor array system. Here, we highlight the ability of the signal capacitive sensor sheet to identify different locations strain arrays. Moreover, capacitance-sensing methods as well as efficient and scalable electronic measurement systems for small capacitance

H. Nesser, G. Lubineau
King Abdullah University of Science and Technology (KAUST)
Physical Sciences and Engineering Division (PSE)
COHMAS Laboratory
Thuwal 23955-6900, Saudi Arabia
E-mail: hussein.nesser@kaust.edu.sa; gilles.lubineau@kaust.edu.sa

The ORCID identification number(s) for the author(s) of this article can be found under https://doi.org/10.1002/aelm.202100190.

DOI: 10.1002/aelm.202100190

variation are reviewed. We introduce commercial capacitance-sensing integrated circuits (ICs) and the methods that consider the capacitive sensor as a lumped equivalent circuit with high electrode resistance and leakage. These methods are considered as computational intelligence when an embedded system based on capacitive strain is released. Under numerous operational conditions, wired connections between a sensor and its IC cannot be established. Capacitive strain sensors are especially important for designing wireless systems for in situ monitoring. Further, we discuss the importance of capacitive sensors in remote sensing without the need for a power source using an oscillating circuit. We address the features, characteristics, and applications of capacitive sensors important for designing novel technologies in various fields. This article comprehensively and concretely summarizes the work related to capacitive strain sensing in recent years. The sensing methods, the electronic interface, the capacitive sensor's ability to detect strain over a large surface down to its use in wireless strain detection are extensively presented for the first time.

2. Mechanisms and Sensitivity

Conventional flexible capacitive sensors consist of a parallel-plate capacitor, which comprises two conformable electrodes with a dielectric layer in-between,[62–64] as presented in **Figure 1**. Stretchable dielectric materials are commonly used as flexible supports for soft strain sensors, such as rubbers (e.g., natural rubber and thermoplastic elastomers (TPEs))[65–71] and silicone-based elastomers (e.g., Ecoflex, Dragon Skin, and polydimethylsiloxane (PDMS)).[72–80] A huge difference in Young modulus between the thin metallic film (gold, aluminum, and platinum) and flexible elastomer or rubber causes cracks and buckling under stretching. The inhomogeneity between these two superposed layers decreases the conductivity of the metallic film.[81,82] Thus, conductive elements for a conventional capacitive sensor are fabricated by designing the geometries of traditional materials, such as percolating network,[83] wavy geometry[84,85] serpentine[86] and helical structure,[87] and mesh shapes.[88] In addition, the flexibility of the electrode can be achieved through the incorporation of conductive materials, such as graphene,[89,90] carbon black,[91] metal nanowires,[60,92] metal nanoparticles,[93] and CNTs,[62,94,95] into a polymer matrix. Recently, some studies introduced secondary fillers to improve the mechanical, chemical, and electrical properties of the stretchable composite electrodes. Yun et al.[96] presented the design, the fabrication process, static and dynamic conductivity analysis, and recent applications of the hybrid filler electrodes. Sometimes, this type of electrode exhibits low conductivity or high resistivity that causes a voltage drop across the sensor length. In this case, the electrode resistance needs to be considered in an equivalent circuit with a variable capacitance. In addition, defects and impurities in the dielectric material establish resistance. The lumped circuit model constitutes the virtual electronic component that represents the conventional capacitive strain sensor, as presented in Figure 1b.

The first mechanism of capacitance variation is based on the geometric effect. If we consider a parallel-plate capacitor with a width (ω_0), initial length (l_0), and thickness d_0 (i.e., the distance between the two electrodes), the initial capacitance can be obtained using the following equation:

$$C_0 = e_0 e_r \frac{\omega_0 l_0}{d_0} \quad (1)$$

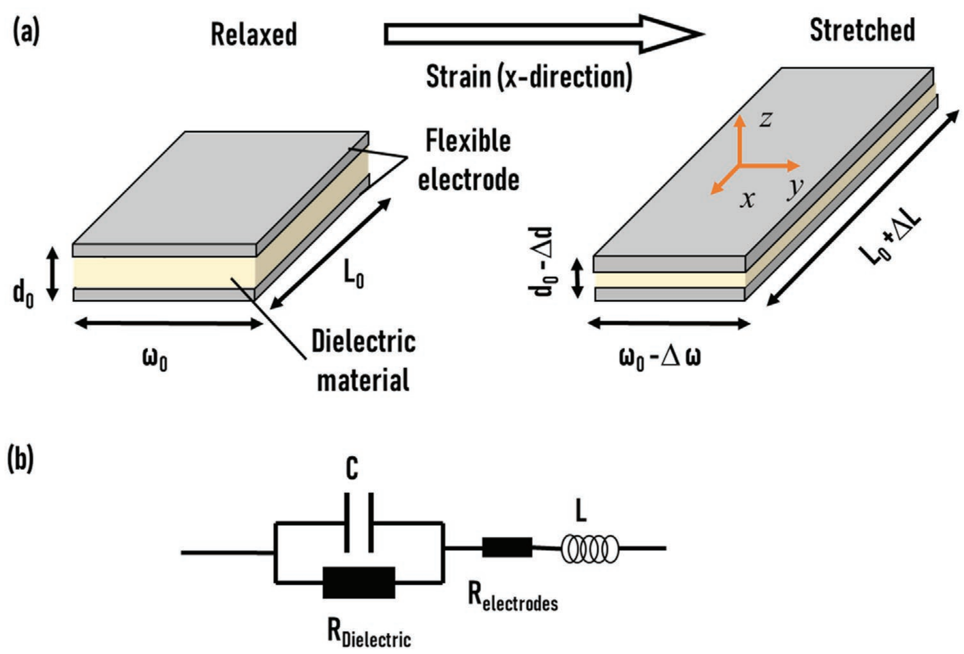

Figure 1. A schematic illustrating the parallel-plate capacitor, where a dielectric layer is sandwiched between two flexible electrodes, a) in a relaxed state and after stretching. b) Typical equivalent circuit for a capacitor. C denotes the central element of the capacitor; $R_{\text{electrodes}}$, the residual resistance of the electrodes; $R_{\text{dielectric}}$, the current leakage in the dielectric material; and L, the inductance in the lead wires.

where e_0 and e_r denote the vacuum permittivity and dielectric constant for the dielectric layer. Under uniaxial strain, ε, the active area of the sensor increases, whereas its thickness decreases due to Poisson's fraction, which results in capacitance variation. In general, the electrode and dielectric material are assumed to have the same Poisson's ratio. Then, the capacitance under stretching is calculated as follows:

$$C = e_0 e_r \frac{(1-\nu\varepsilon)\omega_0(1+\varepsilon)l_0}{(1-\nu\varepsilon)d_0} = C_0(1+\varepsilon) \tag{2}$$

where ν denotes Poisson's ratio for the dielectric layer and stretchable electrodes.

The relationship between the capacitance variation and strain is denoted by GF, which provides the sensitivity of the strain sensor where a high GF is required to distinguish small deformations. The capacitive GF is calculated by dividing the relative capacitance variation by strain, ε:

$$GF = \frac{\Delta C/C_0}{\varepsilon} \tag{3}$$

In theory, the GF associated with the geometric effect in a parallel-plate capacitor strain sensor is 1,[97–106] which is very limited compared with those of resistive strain sensors. Numerous studies have been conducted to investigate capacitive strain sensors based on the geometric mechanism, as presented in **Table 1**. These works mostly focus on the enhancement of the performance of a structure or realization of specific applications. Some studies were aimed at validating a new fabrication technique or type of electrodes exhibiting high stretchability and conductivity.[62,98,99,102,103] Others have demonstrated specific applications, such as developing a particular structure that can be easily integrated into particular locations in the body (finger, elbow, or ankle) for motion tracking.[60,96,100] Other studies have developed high-performance capacitive sensors that exhibit high stretchability, linearity, low hysteresis under cyclic loading, and high repeatability.[62,101] Resistive and capacitive sensors were also compared.[101] Multifunctional sensors that can detect strain, pressure, finger touch, and pressure mapping were developed.[60]

However, some applications, such as electrophysiological signals (pulse, record electromyography, and electrocardiograms), generate very low strain, thus requiring ultra-sensitive sensors. Recently, there has been a dramatic increase in the studies on the improvement of the capacitive strain sensor sensitivity.

In addition to the conventional parallel plate capacitor (**Figure 2**a), researchers create new shapes or modify the mechanical properties of materials to adopt the increasing sensitivity of capacitive strain sensors. For example, Kim et al.[107] fabricated an interdigitated capacitive strain sensor based on AgNW electrodes embedded onto the PDMS substrate (Figure 2b). The interdigitated pattern design achieves higher sensitivity compared with the parallel-plate model as the two electrodes and the dielectric layer are placed in the same plane. When the strain sensor is stretched perpendicularly to the comb direction, the spacing between the comb, d_0, increases to $(1 + \varepsilon) d_0$. However, the initial length, l_0, and the initial thickness, t_0, which are perpendicular to the stretching direction, decrease to $(1 - \nu\varepsilon)l_0$ and $(1 - \nu\varepsilon)t_0$, respectively, due to Poisson's ratio (ν). The below equation expresses the capacitance after stretching as a function of the initial capacitance:

$$C = \frac{(1-\nu\varepsilon)(1-\nu\varepsilon)}{(1+\varepsilon)} C_0 \tag{4}$$

Poisson's ratio increases the GF up to −2.0, exceeding the GF limit for conventional capacitive strain sensors (GF = 1).

Nur et al.[109] proposed a new structure based on a wrinkled electrode film (Figure 2c). They created natural wrinkling in the parallel-plate capacitor to introduce an additional degree of freedom so that a higher sensitivity can be achieved. They modified the classical capacitive formula of the parallel-plate model (Equation (1)) while keeping the dielectric Poisson's ratio in the equation:

$$C = \frac{(1+\varepsilon)}{(1-\nu_{\text{dielectric}}\varepsilon)} C_0 \tag{5}$$

They created this structure by transferring ultrathin gold electrodes to a pre-stretched dielectric layer. They achieved a GF of 3.05, with a stretchability of up to 140% strain with high linearity and negligible hysteresis.

Shintake et al.[108] demonstrated the integration of hierarchical auxetic structures into a flexible capacitive strain sensor to improve sensor sensitivity (Figure 2d). Auxetic arrangements are a type of metamaterial with a negative Poisson's ratio that influences the capacitance upon an applied strain. Unlike the classical parallel-plate sensor, the distance between the electrodes increases when stretching the sensor in its plane. They demonstrated that the sensitivity of the capacitive strain sensor doubled while other characteristics are maintained, such as repeatability, low hysteresis, and high linearity.

Another mechanism working at the nanoscale with nano- or microcapacitance is the acquisition of a considerable number of small capacities that result in capacitance variation at a large scale. Nesser et al.[110] realized a capacitive strain sensor based on gold nanoparticles deposited between interdigitated electrodes on a flexible substrate (Figure 2e). This approach is based on the interparticle electronic coupling. The total capacitance of the nanoparticle assemblies can be derived from the tunnel junctions presented by a parallel R–C electrical model between two metallic nanoparticles. An analytical expression is given for the capacitive GF defined as follows:

$$GF = -\frac{d}{l \ln\left(1+\frac{d}{l}\right)} \tag{6}$$

This model shows a new representation of the capacitance GF that depends on the nanoparticle size (d) and the distance between nanoparticles (l). In the case of 14-nm gold nanoparticles, a GF of approximately −3.5 was obtained.

Yuan et al.[111] reported a new type of nanocomposite material composed of a PDMS matrix charged with reduced graphene

Table 1. State of the art of capacitive strain mechanisms and properties.

Reference	Mechanism	Material and structure	Sensitivity (GF)	Stretchability [%]	Point of interest	Limitation/drawback
[97]	Geometric	AgNWs/Ecoflex	0.99	150	Using finger kinematic tracking	Sensitivity
[98]	Geometric	Silver-buckled surfaces	0.9	80	Increasing the stretchability of metallic electrode by laser rastering of elastomer surface	Sensitivity
[99]	Geometric	Conductive knit fabric/silicone elastomer	1.23	100	Developing a new batch of manufacturing technology (laser cutting) GF > 1 because $\nu_{electrode} < \nu_{dielectric}$	Sensitivity, linearity
[100]	Geometric	Ionically conductive fluid-silicone elastomer	0.34	250	Multicore-shell fiber sensor	Sensitivity, repeatability/lifetime, liquid material
[101]	Geometric	Planar capacitor with carbon black composite	0.98	500	Improving the stretchability and performance compared with the resistive sensor	Sensitivity
[62]	Geometric	PDMS-CNT	1	300	Improving the stretchability, performance, and transparency of the sensor	Sensitivity
[102]	Geometric	Dragonskin-graphite	0.54–1.13	250	Combining screen-printing and direct writing to fabricate the sensor	Sensitivity, accuracy
[103]	Geometric	CNTs-Ecoflex	1	150	Developing a stretchable electrode based on contact-transfer patterning of carbon nanotube forests	Sensitivity
[62]	Geometric	CNTs-silicone elastomer	0.99	100	Developing a high-performance sensor based on stretchable percolated CNT electrode by vacuum filtration	Sensitivity
[60]	Geometric	AgNWs-Ecoflex	0.7	50	Detecting strain, pressure, and finger touch for several wearable applications	Sensitivity
[104]	Geometric	CNT/Ecoflex	0.49	50	Improving the electrode's stretchability. The electrode is a carbon nanotube film deposited by spray coating	Sensitivity
[105]	Geometric	MXene/PVA hydrogel-BHB	0.4	200	Realizing a stretchable electrode with high sensor performances	Sensitivity
[106]	Geometric	Vertical graphene-PDMS	0.97	80	Developing stretchable electrodes based on vertical graphene (VGr)	Sensitivity
[107]	Interdigitated electrode	AgNWs-PDMS	2	30	Improving the GF: Electrode and substrate in the same plane (no influence of Poisson's ratio in the out-of-plane direction)	Linearity, negative variation
[108]	Hierarchical auxetic structures	Silicone/acrylic elastomer-liquid metal	1.61	50	Improving the GF by modifying the mechanical properties	High thickness, limitation on the application
[109]	Wrinkled electrode	PDMS-Au film	3.05	150	Improving the GF by creating a high degree of freedom in the out-of-plane direction	Linearity, hysteresis
[110]	Tunneling junction	Polyimide-Au film/Au NP	3.5	1.5	Improving the GF by using an assembly of nanoparticles (detect low strain)	Low initial capacitive
[111]	Permittivity variation	Silver greases-rGO/PDMS	13.6	4	Improving the GF by creating a microcapacitor with the rGO plate in a PDMS matrix	High electrical loss of dielectric material
[112]	Transmission line model	CNT-PDMS	37	50	Improving the GF by using fragmented and highly resistive electrodes	Need AC voltage
[113]	Planar electrodes	Ionic hydrogels- AgNFs	165	1000	Nanometer-thick EDL	Limitation on the mobility of ions

oxide (rGO) (Figure 2f). The anisotropic flakes were assembled into locally aligned structures, which are liquid crystals with long-range orientational order. Extended microcapacitors that achieve a very high permittivity can be widely formed by this ordered structure. Yuan et al.[111] demonstrated that due to the graphene microcapacitors within the PDMS, this nanocomposite material could induce an enormous change in the permittivity within a small strain range. They obtained a capacitive GF of –13.6 with a decrease in capacitance under applied strain. Another study based on the variation of the permittivity was also developed by establishing a near-percolated network of a conducting filler in an insulating polymer matrix.[114]

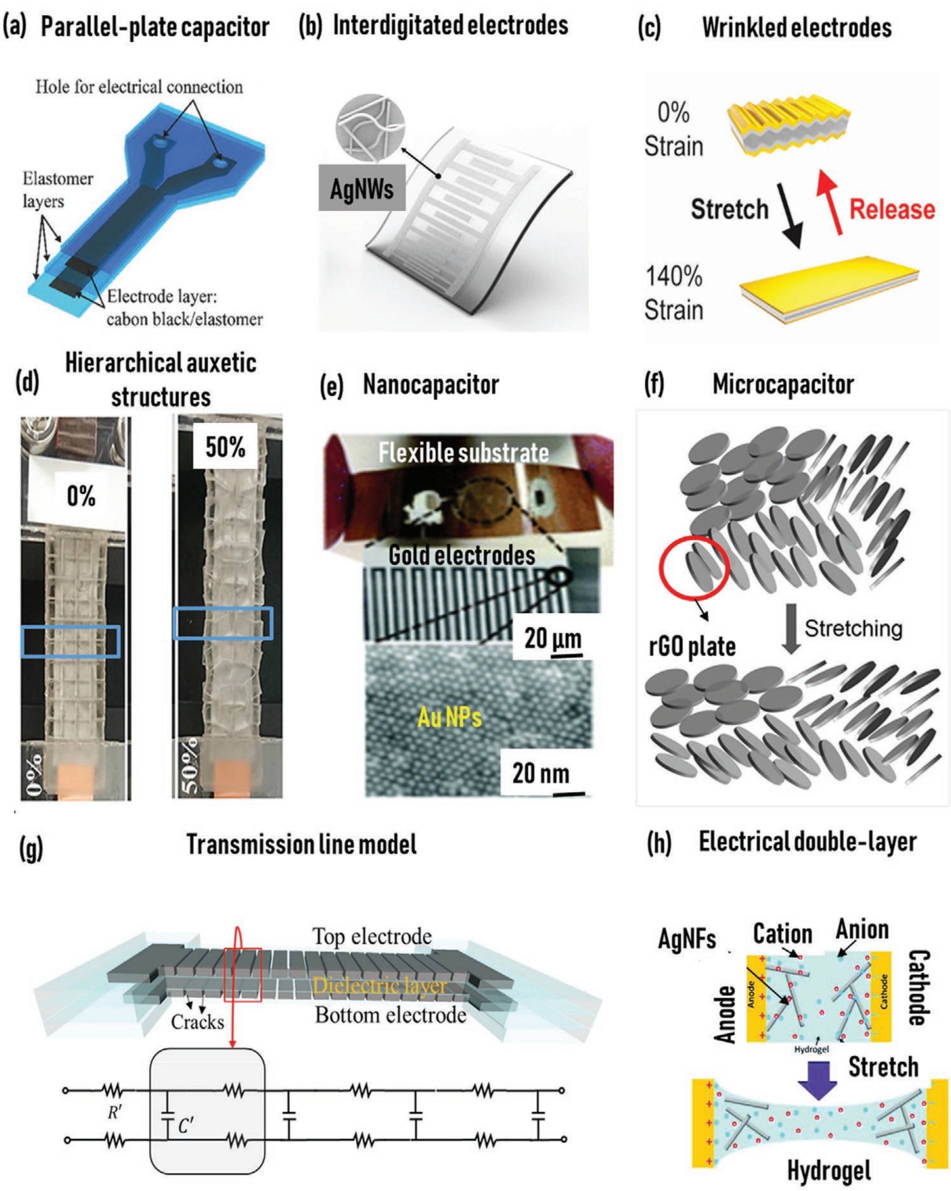

Figure 2. Mechanism of capacitive strain sensor: a) Geometric effect: a parallel-plate capacitor consisting of electrode (carbon black) layers and dielectric layers (elastomer) (GF = 1). Reproduced with permission.[100] Copyright 2018, Wiley-VCH. b) AgNWs/PDMS interdigitated capacitive strain sensor (GF = 2). Reproduced with permission.[107] Copyright 2017, American Chemical Society. c) Ultrathin wrinkled Au film strain sensor before and after stretching (GF = 3.05). Reproduced with permission.[109] Copyright 2018, American Chemical Society. d) Sensor with and without auxetic structure fabricated with elastomer and EGaln (GF = 1.61). Reproduced with permission.[108] Copyright 2019, Frontiers in Robotics and AI. e) Interdigitated electrode including gold nanoparticle assemblies (GF = 3.5). Reproduced with permission.[110] Copyright 2018, The Royal Society of Chemistry. f) Schematic illustrating the distribution of graphene liquid crystal monodomains with and without external strain (GF = 13.6). Reproduced with permission.[111] Copyright 2018, American Chemical Society. g) Fragmented electrode-based sensor as the transmission line model as an infinite series of lumped circuits (GF = 37). Reproduced with permission.[112] Copyright 2021, American Chemical Society. h) Schematic illustration of a hydrogel structure representing the reduction in the electrical double-layer area at the conductive and ionic materials with strain and capacitive reactance change (GF = 165). Reproduced with permission.[113] Copyright 2019, The Royal Society of Chemistry.

A recent study by Nesser et al.[112] presented a new structure based on a dielectric elastomer (DE) layer laminated between two fragmented CNT papers that experience a significant change in resistance (from Ω to MΩ) when stretched (Figure 2g). The capacitance variation results from the penetration of the interrogating signal, which strongly depends on the strain and the interrogating frequency, and is well beyond the classical geometric factor. Based on the transmission line theory, a new relationship between the sensor capacitance and strain is expressed by the following equation:

$$C = \frac{-\ln\left(\frac{V_{\min}}{V_0}\right)}{\sqrt{2\pi f C_0 R_0 \left(\frac{e^{\mu\varepsilon}}{1+\varepsilon}\right)}} C_0 \tag{7}$$

where V_0 denotes the magnitude of the input voltage; V_{min}, the minimum voltage, which is negligible; R_0 and C_0, the initial electrode resistance and capacitance without strain; μ, the GF of the electrode resistance; and f, the frequency of the sensing signal. The high sensitivity of this sensor is demonstrated by a GF exceeding 37 at a strain of 3%.

Interestingly, recent studies have reported new types of capacitive sensors based on electrical double-layer (EDL) structure formed by ionic liquids between two electrodes.[115–118] The EDL structure is formed between the electrodes when they are exposed to an external signal. This approach is based on the accumulation of electrons in metals and ions (opposite polar with electrons). The ultra-large interfacial capacitance is achieved after the appearance of a nanometer-thick EDL, resulting from the interfacing between the ionic hydrogel and metals (electrodes). In this case, the capacitive value of the ion gel between the two electrodes is significant.[119–121] A small variation in dimension induces a considerable variation in capacitance. Based on this mechanism, Xu et al. fabricated a new capacitive strain sensor based on a nanocomposite containing ionic hydrogels and silver nanofibers (AgNFs), as presented in Figure 2h. Under strain, the interface between the hydrogel and metal is reduced, and a variation in capacitance is formed. They achieved a capacitive GF of 165.[113]

With these innovative methods and mechanisms that improve the sensitivity, the traditional GF value of capacitive strain sensors (limited to 1) was exceeded; however, it remained much lower than that of the resistive sensors, which reaches 10^6 for some applications.[38,122] Sometimes, the overlarge GF for resistive stretchable strain sensors yields a large error (50% for some sensors).[123]

3. Achieving Local Detection and Large Area Coverage

Most mechanical sensors can detect pressure, strain, and touch by a single measurement, although the methods vary. Some applications require the distribution of the sensing capability over a large area and recognition of multiple pressures or touchpoints without limitation. Different approaches have been proposed for monitoring strain over a large area, including resistive sensing sheets,[124] series transistor circuits,[125,126] printable conductive polymer,[127] micro-hollow structures,[128,129] electric field tomography,[130] patch antenna sensors,[131,132] and soft elastomeric capacitors.[133–135] Networks of independent sensors[136–139] and arrays of flexible sensing substrates[71,140–145] are typical methods for locally detecting or monitoring large areas with high spatial resolution. In the early stage, touchscreen technologies have been investigated for sensing contact location on a display surface.[146,147] For that, the existing scalable sensors based on conventional technologies are mostly rigid and require a large object that touches the surface. For example, in 2007, Apple has released its first mobile device using multi-touch technology, which used capacitive coupling techniques.[148] Capacitance-sensing technology has been widely studied to obtain a spatially distributed high special resolution over a large area that can reach the limits of square centimeters. The resistance variation was measured in arrays of conductive microchannels[136,149,150] for strain sensing. However, the resistive approach does not provide high performance due to the overlap between cells; however, this drawback is avoided with the capacitive sensor array.

Most artificial skins that are capable of detecting localized deformation while covering a large area consist of an array of distributed pressure and tactile sensors. Several conditions are required for the adoption of large-area sensors in various applications, such as structural health monitoring, robots, and motion detection. They must exhibit sufficient flexibility to cover a 3D area and have an adequate spatial resolution (e.g., when high resolution is needed to manipulate structures) and low overlap between cells, the ability to protect the sensor itself and absorb external impact, and reliable sensor response. The common approach uses two flexible layers with rows and columns of conductive strips separated by a dielectric layer.[149,151–157] The conductive strips on the flexible layers are placed in an orthogonal direction to create pixels at the intersections. Each crossing point of the conductive strips forms a parallel-plate capacitor cell in an array. The compression or stretching of this cell by an external mechanical effect generates capacitance variation in a local cell and can be separately detected using a programmable electronic system.

Figure 3 presents the conceptual diagram of a conventional skin sensor for large-area deployment using a network of multicapacitive array systems. One sensor module in this traditional system consists of an $n \times n$ cell array and connects through interconnection lines. Every capacitive cell is created by an interaction between the lower and upper electrodes that form an array of cells. Figure 3a presents a modular expandable capacitive sensor for robotic skin applications.[158] A sensor module is composed of 16×16 cells with a spatial resolution of 1 mm, where the cell itself is composed of copper electrodes and an air gap encapsulated by a PDMS membrane, forming a parallel-plate capacitor. Other examples demonstrate the construction of the capacitive matrix on a large area presented by Li et al.[151] They fabricated two sets of PDMS microchannels (8×8 channel array) filled with a conductive liquid (eGaIn), forming a capacitance-sensing array (Figure 3b). The entire system has a large area of several square centimeters and can detect strain and pressure distributions over a large area with a 1-mm^{-1} spatial resolution. As the system is extremely flexible, it can readily achieve stretchability higher than 500%, as presented in Figure 3b-ii. The capacitive sensor arrays are now a well-developed technology with multiple commercially available devices (Sensitronics, SureTouch, TakkTiles, Sensing Tex, and BodiTrak Tekscan).

Some examples of capacitive large-area strain, choose according to the application domain, are presented in **Figure 4**, such as making gloves for virtual games (Figure 4a), robotic skin (Figure 4b), following hand and biceps motion (Figure 4c), monitoring cracks in reinforced concrete (Figure 4d) and measuring the reaction of forces in the human body (Figure 4e) monitoring cracks in reinforced concrete (Figure 4e). A soft elastomeric capacitor sensor has been developed to monitor damages in large-area structures.[134] This capacitive sensor network is used in numerous structural health monitoring applications, including the evaluation of wind turbine blades,[159] dynamic nondestructive testing,[160] in-plane strain map

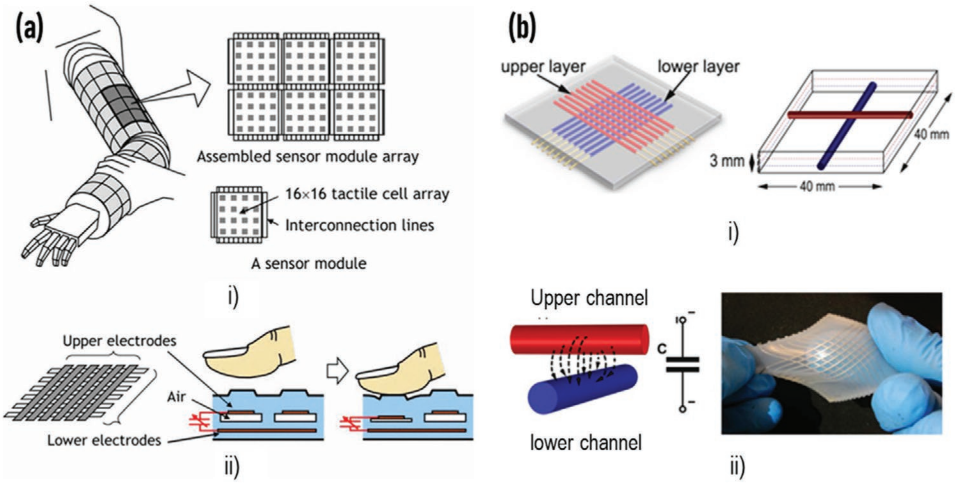

Figure 3. a) Schematic illustrating a conventional large-area capacitive array sensor: i) assembly of module array covering a robot hand, ii) single-cell structure: the intersection between two conductive lines isolated by an air gap, forming the parallel-plate capacitor. Reproduced with permission.[158] Copyright 2006, IEEE. b-i) Typical capacitance-sensing array. ii) Single capacitive element of the sensing array and optical image showing a 4 cm × 4 cm × 3 mm flexible silicone rubber membrane containing 8 × 8 sensor arrays. Reproduced with permission.[151] Copyright 2006, IOP Publishing.

reconstruction,[161] sensing distortion-induced fatigue cracks in steel bridges,[162] and crack detection in a concrete plate.[163] The last two examples are presented in Figure 4d where dense sensor network configurations can monitor the strain and crack of large areas.

In capacitive array systems, the number of pixels per unit length is still limited. For obtaining well-defined pixels, fabricating sensor systems can be complicated and requires accurate patterning. For this reason, new methods are being developed to expand the sensing area using novel fabrication methods or flexible materials. For example, Zhu et al.[170] developed a multi-touch capacitive sensor that can identify multiple touches on different locations using only four independent channels. Their objective was to decry the number of connections and wires on the array systems by combining four capacitive sensors that have partially overlapping areas. This device is convenient for emerging wearable technologies and humanoid devices.

Moreover, a capacitive sensor with a single ion gel layer and copper electrodes was reported by Joon Park et al.[171] for detecting pressure positions, as presented in **Figure 5**a. The electric field variation in the ion gel layer enables pressure detection.[162,172,173] Moving away from the electrodes decreases the electric field, thus influencing the relative capacitance variation at different positions, where the capacitance further decreases, as presented in Figure 5a. Yoon et al.[174] employed a similar principle for detecting localized pressure. They used ionic liquids in microchannels acting as electrodes to realize a microfluidic multifunctional capacitive sensor, where the dielectric layer is the CNT/PDMS composite. The ion is dense near the electrical sensing input, and its concentration decreases along the lateral direction from the electrodes, rendering the capacitance variation nonuniform over the whole area of the structure. Figure 5b presents the capacitance variation that follows finger sliding motions along the sensor. It should be noted that the ionic capacitive sensor can also be implemented as a sheet of distributed sensors (array of sensors) to demonstrate its capability of detecting the location and pressure of touch.[117,152]

Recent articles have proposed a new sensing method for local strain detection within non-ideal capacitive sensors.[175–178] The sensing input attenuates along the capacitive sensor length with high resistive electrodes, leading to the measurement of different regions of the capacitive sensor by changing the sensing frequency. In this method, the sensor behaves as a transmission line. The dielectric sensor can be idealized as a distributed chain of small capacitors and resistors (**Figure 6**a).[178] The resistance of the electrodes significantly affects the distance a sensing signal can reach. The signal distance can also be controlled by increasing the sensing frequency to limit the penetration of the signal into the sensor. As presented in Figure 6b, within the area of a single capacitive sensor body, the relative capacitance variation is affected by the sensing regions created by applying multiple sensing frequencies to the capacitors.[176,177] The use of the transmission line model makes it possible to measure local capacitance variation and, therefore, local pressure within the same sensor sheet. Sonar et al.[175] employed the transmission line model to detect pressure in 2D. Figure 6c presents the pressure location prediction with high accuracy. The advantage of the multifrequency capacitance-sensing approach is that it reduces the number of interfaces and supports electronics compared with discrete sensor arrays and eliminates the need for multiple sensors.

4. Interrogation Circuit and Sensing Methods

Various types of electronic test equipment can be used to measure signals and capture responses from electronic devices under test (DUTs). The capacitance variation of a capacitive sensor is generally on the order of pF; this value can be measured using a conventional capacitance meter, LCR meter, or impedance analyzer. The replacement of this macroscale

ADVANCED ELECTRONIC MATERIALS
www.advelectronicmat.de

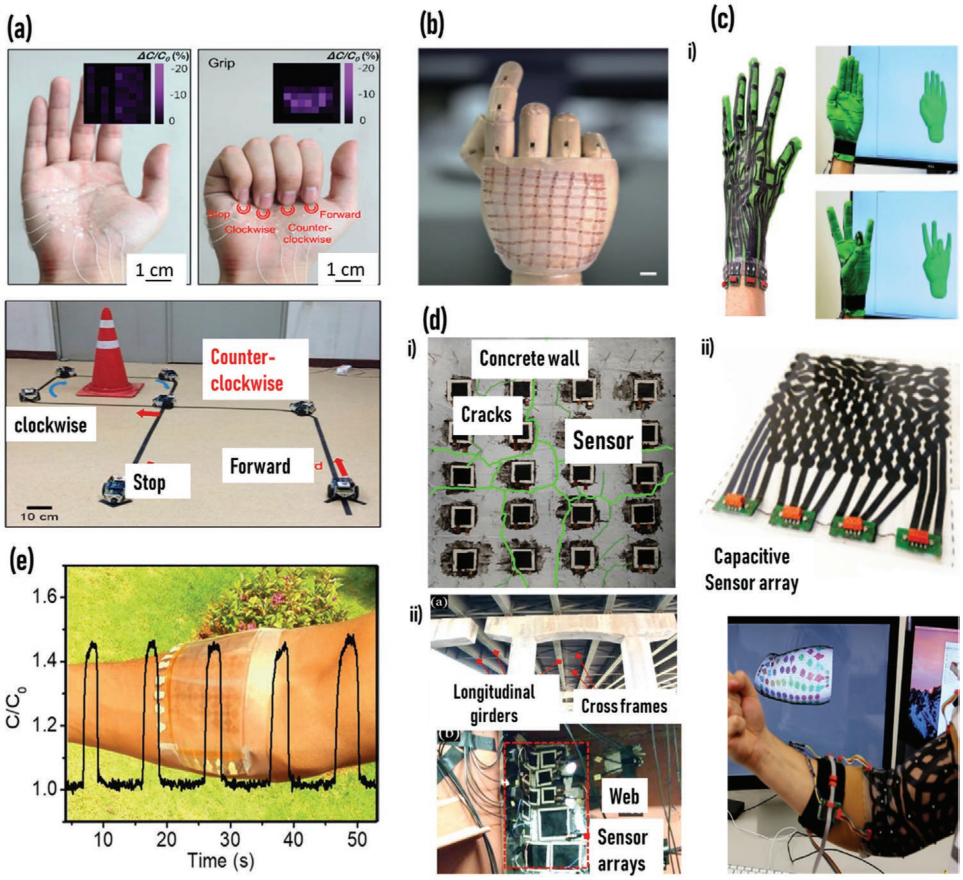

Figure 4. Large-area strain covering for various applications: a) Gaming: capacitance-sensing array mounted on a palm for remote-controlling a toy car. The inset of each image shows a contrast diagram of relative capacitance variation for open (left) and closed (right) hand Reproduced with permission.[164] Copyright 2017, American Chemical Society. b) Schematic illustration of a capacitive sensor array system as an artificial electronic skin on a hand (scale bar: 1 cm). Reproduced with permission.[165] Copyright 2019, Nature Research. c) Motion capture: i) glove based on a stretchable capacitive silicone sensor array capturing hand poses in real-time with high accuracy. Reproduced with permission.[166] Copyright 2019, Association for Computing Machinery. ii) Flexible capacitive sensor arrays composed of 92 sensor cells, forming an extensive area sensing system and live capturing of the biceps with silicone-based capacitive sensor arrays. Reproduced with permission.[167] Copyright 2019, Association for Computing Machinery. d) Structural health monitoring: i) network of capacitive sensors implemented on the back of the cement-paste plate where thick and thin green lines highlight the cracks. Reproduced with permission.[163] Copyright 2018, International Society for Optics and Photonics, ii) optical image of steel bridges implanted with a dense capacitive sensor array for monitoring distortion-induced fatigue cracks. Reproduced with permission.[168] Copyright 2018, International Society for Optics and Photonics. e) Health monitoring: Capacitive touch panel with 5 × 7 pixels deposited on the arm to monitor external touch with high resolution. Reproduced with permission.[169] Copyright 2019, American Chemical Society.

expensive equipment with a small interface circuit became increasingly attractive in numerous consumer applications. As a definition, an interface circuit is a signal conditioning circuit used to bring the signal from the sensor to a format compatible with the load device or read out the data for a display system. For such capacitive sensors, reading a capacitive difference is the fundamental function of an interface circuit. A conventional electronic system used for the capacitive sensor consists of a capacitive measurement circuit, microprocessor, or microcontroller (μC), in addition to an analog-to-digital converter (ADC), digital-to-analog converter, and memory. A typical block diagram of sensor elements, including the electronic interface, is presented in **Figure 7**. In either case, an IC is at the heart of the product designed to perform real-time computing. The electrical signal detected from the sensor can be wirelessly sent to the interface circuit.

Figure 8 shows some examples of the capacitance measurement circuit starting with the conventional capacitance-measuring method that is based on injecting an input signal to the sensor and recovering the output variation of the signal in the form of voltage, current, pulse-width variation, or frequency. In this configuration (Figure 8a), the capacitance variation represented by the voltage or current signal transforms into a digital word via an additional ADC. Several series of circuits that can measure small capacitive variations have been developed and commercialized in the last few years, including the capacitance-to-digital converter (CDC). The sigma-delta (Σ–Δ) conversion technology is one of the sensing methods developed for a precision capacitive sensor interface circuit.[179,180] Figure 8b presents the structure of a conventional first-order Σ–Δ converter consisting of a switched-capacitor modulator with a digital filter. Over time, this converter balances a known reference charge of variable polarity with an unknown charge.[181] Moreover, the successive approximation register (SAR) is a capacitance-measuring technique used in the CDC and is well known for its excellent energy efficiency.[182–185]

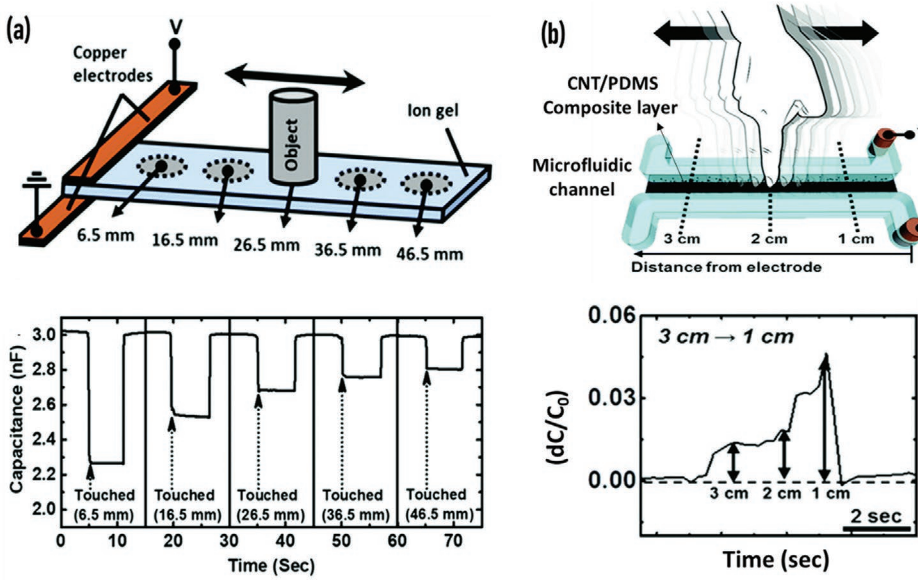

Figure 5. a) Schematic of the signal-layer ionic gel sensor for detecting local pressure where an external object is pressed on a specific position, the graph showing the capacitance variation in real-time for the single-layer ionic gel sensor, depending on the pressing position. Reproduced with permission.[171] Copyright 2019, Royal Society of Chemistry. b) Schematic of microfluidic capacitive sensors pressed in a different location, the graph shows the relative capacitance changes of microfluidic capacitive sensors with finger sliding. Reproduced with permission.[174] Copyright 2017, Royal Society of Chemistry.

Figure 8c presents an example of CDC implementation based on a capacitive array of a SAR ADC connected to a capacitive sensor (C). C is measured by compensating it with the digital input of the programmable capacitor array (C_R), which is adjusted using the SAR logic where the resolution is determined through the smallest capacitor unit in the array.

Reverter et al.[187] proposed a simple capacitance-sensing method where the direct capacitance-to-digital conversion is based on timing and voltage comparison. They connect an RC circuit, including the capacitive sensor, to a µC that calculates the charging and discharging time where the capacitance can be deduced (Figure 8d).

Dietz et al.[189] proposed an alternative sensing method based on charge transfer. Figure 8e presents the implementation circuit of the charge-transfer method and its operating principle, where V_S denotes the source voltage; C_r, the reference capacitance; and C, the unknown capacitance.[188] The sensor capacitance can be identified by counting the number of charge-transfer cycles required to charge the reference capacitance to a threshold voltage through the capacitive sensor.

The µC itself can act as a CDC for the measurement of capacitive sensors without any external component. Some µC contains internal capacitance and analog-to-digital voltage conversion, allowing them to act as a charge-transfer circuit. The direct connection of the capacitive sensor to a µC is the simplest way to implement an interfacing circuit for capacitive sensors.[110]

Numerous CDC converters based on these techniques exist on the market. The "analog" system developed several CDC models frequently used for measuring small capacitance variation, including AD7745,[190] AD7147,[191–193] AD7152,[194–196] and AD7746.[197] **Figure 9** presents some examples of flexible capacitive sensors used in the conventional capacitance-measuring circuit to calculate pure capacitance. Figure 9a presents the packaging of an interface circuit of a capacitive wearable sensing system comprising of a group of capacitive strain sensors to monitor the joint movement of the human body. In this example, the authors use a 24-bit CDC (Analog AD7746) with a 32-bit microcontroller IC (STM32) as an interface circuit.[198] The commercial CDC chips were utilized in various capacitive strain applications to convert sensor capacitance levels to a digital signal. The CDC (AD7147, Analog Devices) was used by Guo et al.[145] (Figure 8b) on a portable measurement system for planar pressure distribution with a wireless transmission module. Gerratt et al.[145] interfaced a 16-bit CDC (AD7147, Analog Devices) with a stretchable capacitive tactile sensor skin for a dorsal side of a robotic hand, where the CDC is integrated on custom printed circuit boards (PCBs), as presented in Figure 9c.

We can find other types of ICs that can be used for measuring capacitance as MPR121 (NXP Semiconductor), an off-the-shelf component intended for use in 12-digit-style capacitive touchpads and keypads. This chip was used by Farrow et al.[146] and was integrated into a flexible PCB to detect the capacitance variation in a soft capacitance array (Figure 9e).

Some sensing boards that are capable of wirelessly transmitting data to the display system have been designed. As presented in Figure 9d, the PCB connected to five flexible capacitive sensors can send data about capacitance to a Bluetooth-enabled device. Then, a mobile application translates the data to give the user information about the hand motion, thus resulting in a smart wireless glove that can detect hand motion, as realized by StretchSense.[200] Yang et al.[201] present a novel wireless transmission data system based on an effective bridge-type impedance readout circuit. By using an on-board microcontroller, the sensor signal is read out locally and transmitted wirelessly. This electronic system is able to measure capacitance and resistance over a wide temperature range (20–180 °C) and

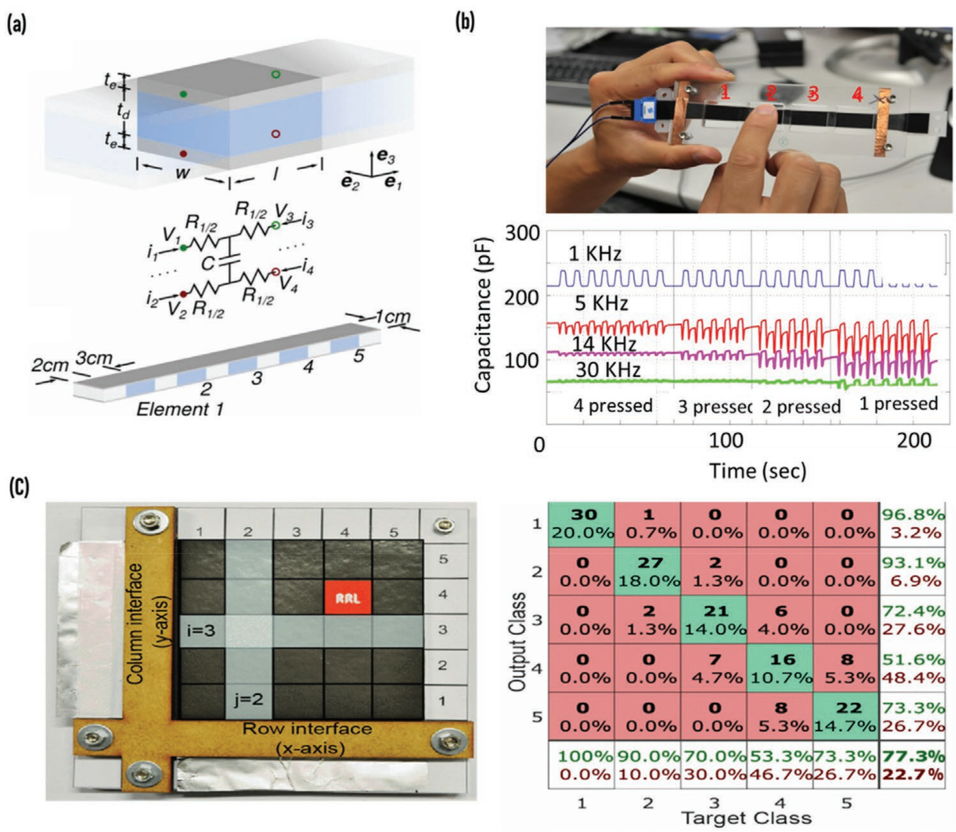

Figure 6. Local strain detection by the transmission line model: a) schematic illustrating the principle of local pressure detection using the transmission line model. The sensor considers an infinite chain of capacitor and resistor segments where l and w are the length and weight of one segment, and the electrode and dielectric thicknesses are t_e and t_d, respectively. Reproduced with permission.[178] Copyright 2017, IEEE. b) Capacitance variation for a different pressed zone in high-resistance dielectric capacitor for different sensing signal frequencies. Reproduced with permission.[177] Copyright 2016, Wiley Periodicals. c) Image representing 2D dielectric capacitive sensor segmented into 5 × 5 pixel sensor with a pressure applicator and the Confusion matrices for 5 × 5 sensor configurations after treatment using a multi-class support vector machine. Reproduced with permission.[175] Copyright 2018, IEEE.

various dielectric mediums (e.g., air, epoxies). This circuit can be used as an electronic interface for sensor systems requiring in situ, continuous impedance measurements.

The example presented in Figure 9f demonstrates how the capacitance of each cell of a large-area capacitive sensor array can be measured with a small interface circuit. One selected tactile sensor is charged by a voltage V_{step} before transferring its stored charge to the feedback capacitance (C_f). It should be noted that a row decoder makes the input selection, whereas a column decoder selects the output cell. Finally, the output voltage is recorded using the equation presented in Figure 9f.[163] The number of channels in the capacitive array sensing system can be increased by combining them with multiplexers, through which some of the commercial CDCs have 256 channels.[169,202]

Other measurement methods were employed to calculate a pure capacitor with a small-scale circuit; for example, Figure 9g presents a complete measurement setup for a soft capacitive sensor realized by Glauser et al.[167] In this measurement, the sensing circuit based on NE555 timer IC has indirectly measured the capacitance by timing the charging of a capacitor to a threshold voltage since the charging time is linearly

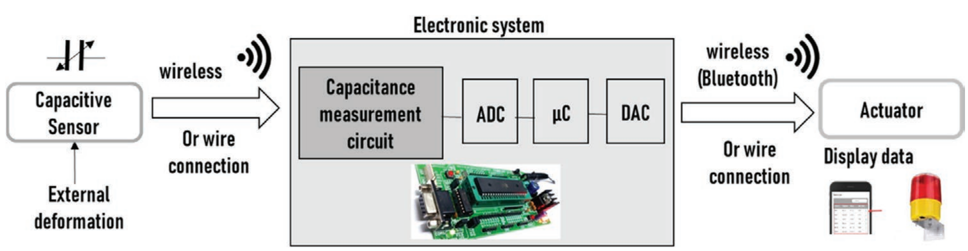

Figure 7. Classical block diagram of the capacitive sensor system, recovering a mechanical deformation from the environment by a sensor, exploiting the signal by an electronic interface, and finishing by displaying information for the recipient.

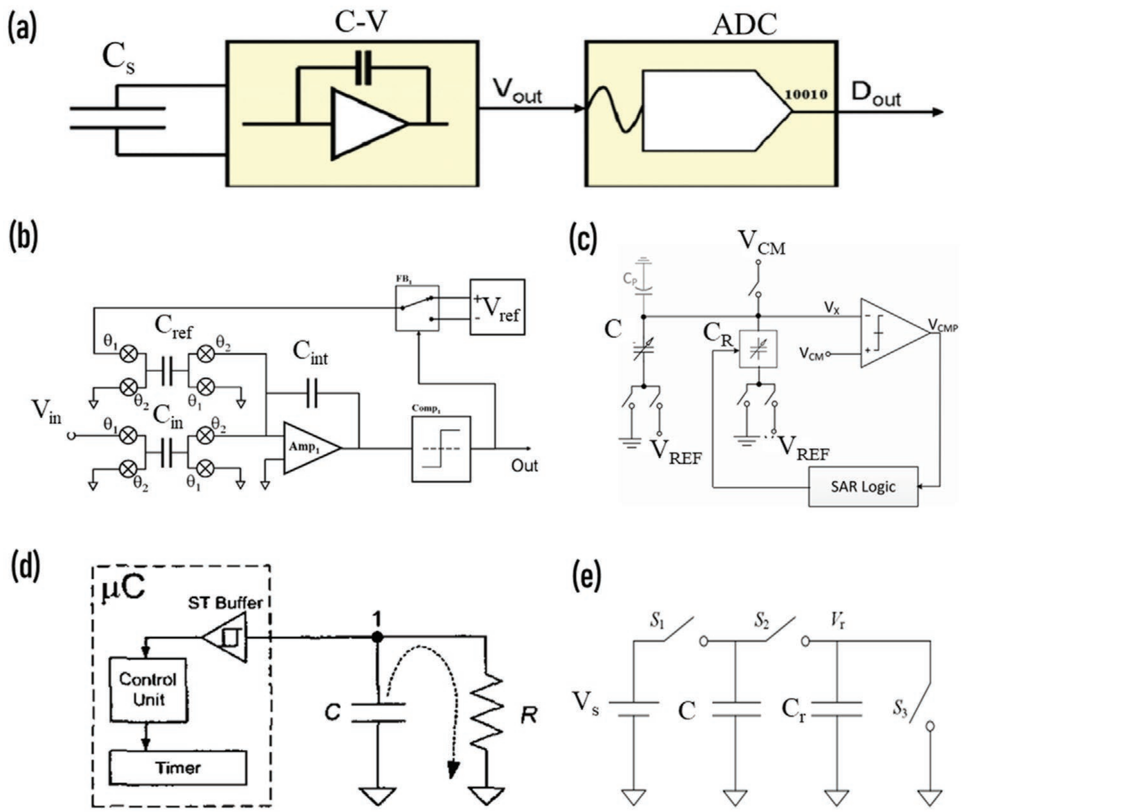

Figure 8. Capacitance measurement circuit: a) typical capacitive sensor interfacing method, b) simplified 1st order Σ–Δ modulator: an integrator adds the charge from the input leg and the reference leg, where the feedback loop contains the integrator. Reproduced with permission.[186] Copyright 2005, IEEE. c) Simplified schematic of a capacitance-to-digital converter using a successive approximation register. Reproduced with permission.[184] Copyright 2014, IEEE. d) Charge and discharge method with a microcontroller interface suitable for measuring low capacitive values. Reproduced with permission.[187] Copyright 2004, IEEE. e) Fundamental circuit representing the charge-transfer method, where V_S denotes the source voltage; C_r, the reference capacitance; and C_x, the unknown capacitance. Reproduced with permission.[188] Copyright 2007, IEEE.

proportional to the capacitance. Then, the square signal of the charging time is read by a µC and transmitted to a display system.

In the selection of a suitable measurement method, several factors are considered, such as the required accuracy, allowed size of the circuit board, and minimum capacitance to be read. Notably, all models presented above neglect the influence of the electrode resistance and function with a direct current (DC) signal. Furthermore, the high electrode resistance of some sensors with low-cost DEs renders most of the commercial capacitance-sensing ICs useless and unsuitable for the measurement of capacitance. Unlike the pure capacitive sensor, the dielectric capacitive strain sensor requires specialized sensing hardware and algorithms to detect and measure the capacitance from a complex circuit model. Therefore, to accurately measure the capacitance, some researchers have developed new methods that consider the resistance of the electrode and its variation under deformation.

Electrical models have been proposed to accurately measure capacitance by considering the electrode resistance (series RC model) and leakage current through the dielectric membrane (parallel RC model) or using the combination of the two models with a lumped model,[202–204] as presented in Figure 1b. One of the popular sensing methods typically employed by numerous commercial LCR meters is the gain and phase method.[205,206] This method is based on the measurement of the current gain and phase shift in a series RC model with regard to the sinusoidal sensing voltage; the gain and phase shift occurs due to the presence of the electrode resistance ($R_{\text{electrodes}}$). The measurement of complex electrical impedance of the sensor's equivalent circuit Z allows capacitance (C) to be calculated by simultaneously solving the magnitude and phase of the impedance equation:

$$Z(j\omega) = \frac{I(j\omega)}{V(j\omega)} = R_{\text{electrodes}} + \frac{1}{jC\omega} \tag{8}$$

Several researchers in the field of self-sensing of dielectric actuators have employed this technique to measure the capacitance, as it is considered to be a robust way to account for the electrode resistance for a dielectric capacitor with low-cost carbon electrodes.[71,154,207,208]

Jung et al.[209] and York et al.[210] developed another measuring method that requires the measurement of impedance along with a wide range of frequencies. The capacitive DE actuator is placed in series with an external resistor, where the output voltage is measured by treating the circuit as a high-pass filter (**Figure 10**a). By calculating the cutoff frequency, the

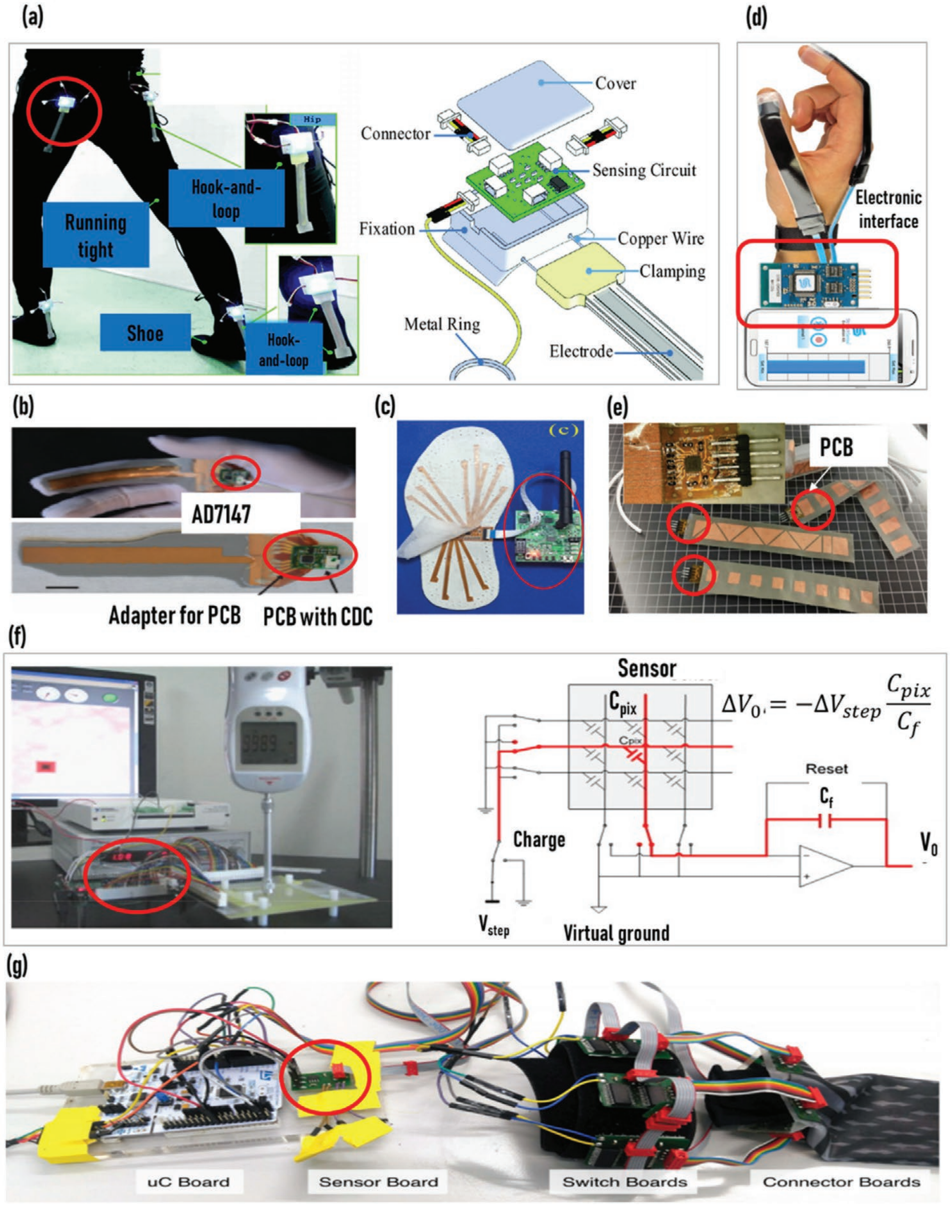

Figure 9. Capacitive strain sensor with their electronic interface circuit: a) capacitive strain sensors and electronic interface control integrated on several joints in a human body to capture motion and the installation of the sensing circuit. Reproduced with permission.[198] Copyright 2019, Springer. b) Image showing a small integrated electronic board that contains a capacitance-to-digital converter (the scale bar is 1 cm), managing the electrical signal of the capacitive sensor. Reproduced with permission.[145] Copyright 2015, Wiley-VCH. c) Network of pressure sensors integrated into plantar shoes and connected to a signal acquisition circuit. Reproduced with permission.[199] Copyright 2016, IOP Publishing. d) Smart glove to monitor hand motion, where a small PCB is used to read the electrical signal of the sensor and send the data to a mobile application via Bluetooth. Reproduced with permission.[200] Copyright 2021, StretchSense. e) Collection of functionalized soft capacitive sensor connected to a very small polyimide flexible printed circuit board (PCB). Reproduced with permission.[146] Copyright 2017, IEEE. f) Measurement setup and schematic representation of readout circuits for capacitive tactile sensor array. Reproduced with permission.[163] Copyright 2009, Elsevier. g) Modular measurement setup of flexible capacitive sensor arrays showing a microcontroller and sensing board in addition to switchboards. Reproduced with permission.[167] Copyright 2019, Association for Computing Machinery.

capacitance variation that shifts the output voltage magnitude of the high-pass filter can be deduced. The cutoff frequency (f_c) of a high-pass filter is inversely proportional to the capacitance (C):

$$f_c = \frac{1}{2\pi RC} \tag{9}$$

Figure 10a demonstrates self-sensing of the DE actuator based on the high-pass filter method. The expansion of the DE actuator increases the capacitance from C_1 to C_2, resulting in a cutoff frequency shift from f_{C1} to f_{C2}. Thus, the voltage variation achieved at a fixed frequency can be used to measure the variation in capacitance.

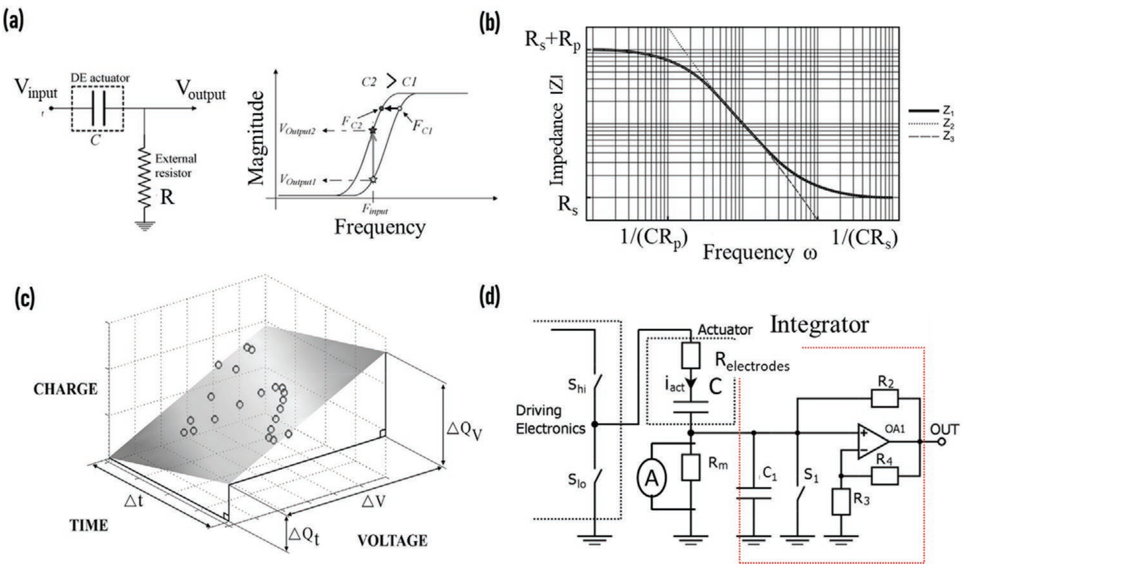

Figure 10. Sensing methods of the capacitive sensor with high electrode resistance: a) high-pass filter method: equivalent circuit of a dielectric actuator connected to an external resistor forming a high-pass filter; the graph shows the cutoff frequency and magnitude shift when the actuator expands. Reproduced with permission.[209] Copyright 2008, Elsevier. b) Schematic plot of the frequency-dependent impedance; the impedance frequency sweep is used to deduce the capacitance value (R_s and R_p are the series and parallel electrode resistance respectively). Reproduced with permission.[211] Copyright 2013, IOP Publishing. c) Hyperplane method: 3D graph representing the relationship among voltage, charge, and time data and fitted with a 2D hyperplane. This plan projection in the V–Q axis is used to determine the capacitance value. Reproduced with permission.[212] Copyright 2013, American Institute of Physics. d) Sensing circuit of the current integration method: dielectric actuator connected to an integrator and switching matrix. Reproduced with permission.[213] Copyright 2011, International Society for Optics and Photonics.

Modeling the impedance frequency response curve is an alternative method employed for calculating the capacitance of DE sensors or actuators.[202,211,214,215] As presented in Figure 10b, Haus et al.[211] demonstrated that the particular points in a simple impedance–frequency curve can be utilized to deduce the capacitance and other parameters of the lumped circuit. At high frequencies, the lumped model reduces to only its series electrode resistance (Rs) as the impedance of the capacitive element in the DE (Xc) approaches zero (Xc→0). Contrarily, at low frequencies, Xc drops out of the lumped model because it approaches infinity (Xc→∞). The inconstant impedance of the lumped model results from the relationship between Xc and frequency. Based on this assumption, all the parameters of the lumped model can be concluded with the following features: the 3dB cutoff frequency response, low frequency, and high frequency.

A new method known as hyperplane approximation was developed by Gisby et al.,[212] which is also based on the lumped model. This method is one of the algorithms used for calculating the capacitance that precisely compensates for the leakage current and resistance of the electrodes. Here, the capacitance is calculated using Cramer's rule by performing a linear regression on the sensor's charge (Q), voltage (V), and current (I) over a given period (T) of the input sensing signal. Analytically, the charge (Q) of a non-ideal capacitor cannot be just represented as the charge stored in the sensor's capacitive component (C), but the charge leaked through the membrane (Q_{leakage}) will add to it. We should note that part of the total sensor voltage (V) is dropped across the electrode resistance ($R_{\text{electrodes}}$), where the capacitive component receives the rest of the total voltage (V_c).

$$Q = CV - CR_{\text{electrodes}} I + \frac{\partial Q_{\text{leakage}}}{\partial t} T \tag{10}$$

In this case, the capacitance of the sensor can be deducted by the gradient $C = \frac{\partial Q}{\partial V}$ of the total charge. On the other hand, it can be represented by the best curve-fitting on the Q–V plane (Figure 10c). Using this method, Xu et al.[216] designed an interface circuit to simultaneously measure multiple capacitive strain sensors.

Matysek et al.[213] employed a simple method for self-sensing the dielectric actuator. The current integration method is based on a transient effect when charging the actuator. According to their work, the capacitance can be calculated using the basic capacitance equation that relates the charge (Q) and the voltage across the capacitance (V_c) with the capacitance (Equation (11)). Further, the supply square voltage (V_s) applied to the actuator is different from the voltage across the capacitance only (V_C) as the actuator is represented by a resistance ($R_{\text{electrodes}}$) in series to the capacitance (C). To calculate the V_c value, the method proposes to wait 3 RC time constants until the capacitance component is fully charged, and V_c equals the supply voltage, V_s. The quantity of charge stored on the capacitive component is calculated by integrating the current passing through the DE. This current is similar to the current flow into $R_{m,}$ which facilitates the measurement, as presented in Figure 10d. In this case, the capacitance is expressed as follows:

$$C = \frac{Q}{V_c} = \frac{\int I dt}{V_s} \tag{11}$$

The current integration can be realized using a hardware element by implementing the Deboo single-supply integrator on the sensing circuit, as presented in Figure 10d. Xu et al.[217] modified this method using a constant DC voltage instead of the square wave sensing voltage to continuously track the charge movement to and from the sensors. With this modification, the method avoids the waiting time required to fully charge the capacitor and the losses caused by the resistive electrode.

5. Wireless Communication between the Capacitive Sensor and Interface Circuit

In some applications, the direct integration of an all-strain sensor package (sensor, cable, and interface circuit) is difficult. The wires that connect the sensors with the interface circuit render the system complex and prevent it from being flexible and independent. Furthermore, the electronic interface is generally rigid, making it susceptible to mechanical failure integrated into a single substrate with a flexible sensor or exposed to external strain. As a result, an inappropriate position of the rigid circuit interface and the wired connection can reduce the lifetime and reliability of the flexible sensor system. These applications include sensing under harsh environmental conditions,[218] sensing moving or rotating parts,[219,220] creak detection in structures and composites,[139,215,221] and medical sensing inside the human body.[222,223] To avoid delamination and mechanical failure in the system, a physical separation between the stretchable sensors and silicon readout circuit communication is required via wireless networking. Therefore, the remoteness of the fragile electronic interface and elimination of its direct presence in the application may be required. Bluetooth Low Energy is a well-known wireless communication system that allows two separate electronic systems to communicate with each other and transfer data. Bluetooth can transmit information fast over a distance of 9 m, making it suitable for durable wearing and multifunctional sensing.[224] As presented in **Figure 11**a, a Bluetooth transceiver needs to be assembled with a rigid IC and rechargeable battery on a PCB. The addition of the battery of the sensor unit and the mechanical stiffness of the Bluetooth module makes the system unfavorable for flexible applications. Unlike Bluetooth, which is an active wireless system, near-field communication (NFC) is a wireless technology that simultaneously enables the transfer of power and data.[225–227] The passive components of the NFC wireless system include a discrete rigid IC that limits the flexibility, as presented in Figure 11b.[226] NFC technology has a maximum delivery distance of about 10 cm, although it offers lightweight and low power consumption. This method also has limitations in terms of rigidity due to the presence of a rigid IC on both the transmitter and receiver sides, thus limiting its applicability to flexible electronics. Unlike stretchable sensor systems that use Bluetooth and NFC technology, passive radio frequency identification (RFID) technology is entirely free from rigid silicon chips and batteries inside the on-application soft sensor tags, thus improving the robustness and conformability of the sensor unit. The sensing system comprises two physically separated parts that are wirelessly coupled using RFID: a stretchable integrated sensor (transmitter) and a readout circuit (receiver) (Figure 11c).[228]

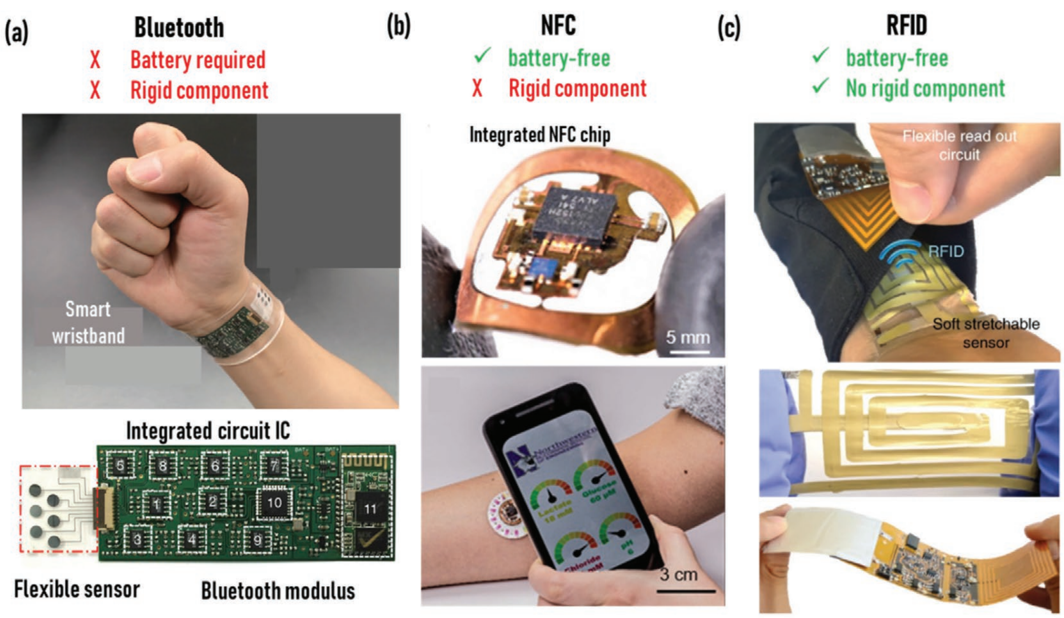

Figure 11. a) Bluetooth communication: image of a Bluetooth system integrated into a flexible and wearable PCB module used with an electrochemical sensor for human sweat analysis. Reproduced with permission.[224] Copyright 2016, Nature Research. b) Near-field communication (NFC): image of a battery-free NFC sensor patch that includes a rigid IC, where the sensor communicates wirelessly with a phone interface. Reproduced with permission.[226] Copyright 2019, American Association for the Advancement of Science. c) RFID wireless communication: image of a readout composed of a flexible printed circuit board on clothes and separated LC stretchable sensor integrated in the skin. This technology is based on an LC oscillator suitable for use as a capacitive strain sensor. Reproduced with permission.[228] Copyright 2019, Nature Research.

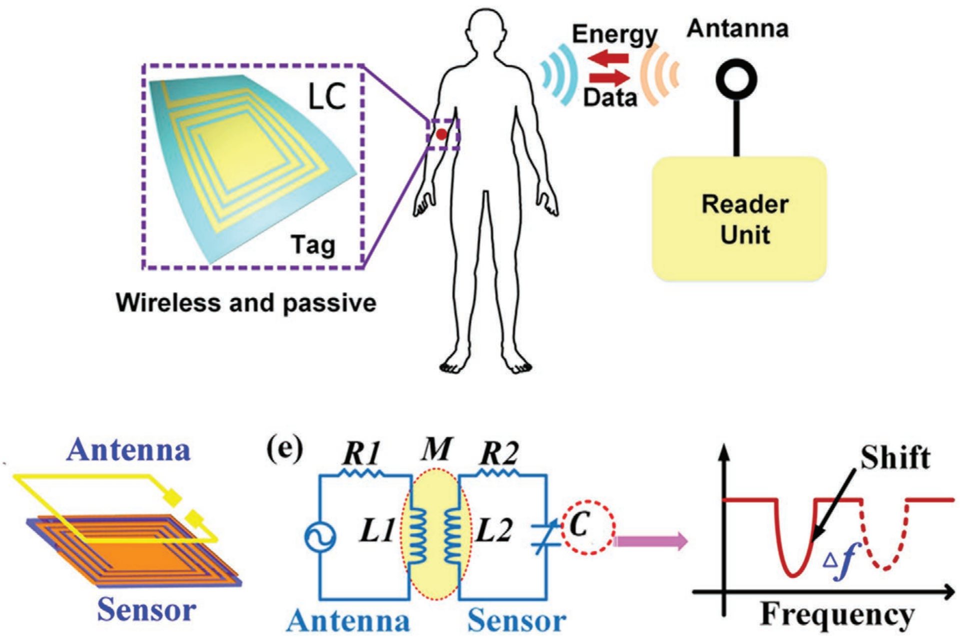

Figure 12. Schematic diagram of a conventional passive wireless sensor based on LC resonators demonstrating how the data and energy can be remotely transmitted from a flexible tag and received by an external antenna. The equivalent circuit shows the Wireless communication principle between the tag flexible sensor and the readout antenna. Reproduced with permission.[229] Copyright 2019, Nature Research.

Figure 12 presents the working principle of the wireless capacitive strain sensor based on RFID technology.[229] In general, the soft tag is made using a stretchable inductor and capacitive sensor to form an inductor-capacitor (LC) oscillator circuit.[230–232] The data transfer between the tag's inductor and the external readout coil is based on electromagnetic coupling, where power transmission is achieved by the inductive coupling of the transformer. The resonant frequency (f_0) of a resonator circuit is expressed[231] as follows:

$$f_0 = \frac{1}{2\pi\sqrt{L_2 C}} \tag{12}$$

where C and L_2 are the capacitance and inductance of the sensor tag, respectively. According to Equation (12) and Figure 12, a shift in electric resonance frequency can be read when the capacitance of the sensor changes. To wirelessly investigate the *LC* sensor, its resonance frequency is monitored by measuring the return loss (S_{11} parameter) of the external readout coil or by following the impedance of the LC sensor. The resonance frequency appears when the sensor absorbs most of the electromagnetic energy, which is demonstrated by an inversed peak in the input return loss, S_{11}. Therefore, the resonance frequency can be remotely deduced from the minimum value of S_{11} with a frequency range. This wireless method is suitable for the capacitive strain sensor due to the capacitive behavior of the sensor under strain. The capacitive strain sensor can be easily converted to an LC wireless sensor by connecting the capacitive strain sensor using a flat spiral coil. Thus, the simplicity in fabricating flexible LC oscillators is an essential advantage for the establishment of a soft wireless sensor. Although most of the existing flexible wireless strain/pressure sensors rely on capacitance changes in the LC passive design, the mechanism of some sensors can be inductive-based mechanical sensing, which depends on inductance changes under mechanical deformation.[233–235] Contrarily, the LC circuit can be connected to an external resistive strain sensor to form an RLC circuit, where the resistance is the operating parameter under strain. In this case, wireless detection is achieved by the quality factor instead of the resonance frequency, depending on the three parameters.[228]

The passive LC sensors have been proposed for the measurement of pressure,[235–238] temperature,[239,240] humidity,[238,241,242] strain,[243–246] and chemical sensing.[247] In addition, a versatile approach based on multiple LC resonators was established for simultaneously monitoring multiple parameters (e.g., temperature, pressure, and humidity).[248,249] All of these sensors share the same concept of wireless detection, where the capacitance or inductance is influenced by the quantity to be measured, which results in a shift in the resonance frequency of the LC circuit. An LC sensor has been considered effective in detecting mechanical effects in a sealed environment, such as tires and harsh environments, as well as in high-temperature applications, such as compressors and turbine engines. Moreover, this wireless sensing system is mainly used in the human body for the purposes of health monitoring and biomedical implants. The first wireless pressure sensor was developed for monitoring intraocular pressure (IOP);[232] since then, numerous implantable sensors have been developed for various biomedical applications. Chen et al.[250] have created implantable wireless pressure sensors for patients with glaucoma and continuously monitored the IOP. This sensor consists of a sensitive pressure capacitor embedded in a deformable diaphragm chamber and connected to a planer inductor fabricated using a spiral metal wire and supported with a flexible disk substrate. An external readout coil can detect pressure in a distance

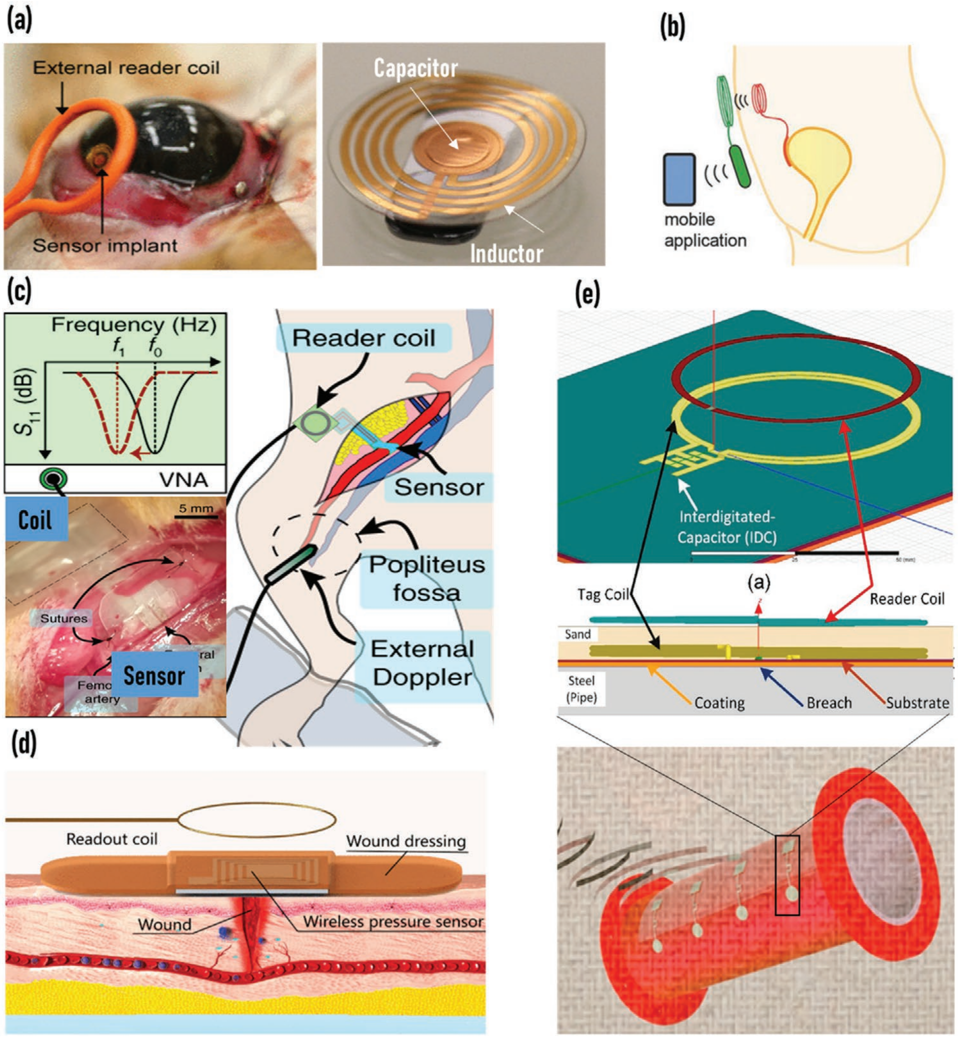

Figure 13. a) Intraocular pressure (IOP) monitoring for the rabbit model using LC wireless pressure sensor; the image on the right shows the capacitor and the inductor parts of the sensor. Reproduced with permission.[250] Copyright 2010, IEEE. b) Schematic illustration of an LC wireless strain sensor implemented on the human bladder to measure large tissue deformations. Reproduced with permission.[251] Copyright 2018, Wiley-VCH. c) Schematic of wireless biodegradable sensors for measuring the arterial blood flow and detecting arterial occlusion. Reproduced with permission.[252] Copyright 2019, Nature Research. d) Schematic illustration of an LC wireless pressure sensor embedded in the wound dressing for monitoring neovascularization and cellular proliferation. Reproduced with permission.[238] Copyright 2018, IEEE. e) LC sensor integrated on a pipeline for monitoring gas diffusion or water ingress: resonant frequency comparison for water- and air-filled gap volume for different breaching heights. Reproduced with permission.[253] Copyright 2017, Elsevier.

longer than 2 cm with a 1-mmHg resolution, as presented in **Figure 13**a. Recently, Kouhani et al.[242] realized a passive sensor implemented inside a contact lens to monitor, in real-time, the curvature of the cornea due to IOP fluctuations.

Other types of applications have been established to target different medical problems. For example, Stauffer et al.[251] reported a wireless strain sensor for monitoring bladder volume (Figure 13b). The implantable strain sensor consists of a coil connected to a stretchable plate capacitor that forms an oscillating circuit. Stauffer et al.[242] validated the concept by implementing the sensor on an in vivo porcine bladder.

Boutry et al.[252] realized an LC pressure sensor to remotely measure the arterial blood flow. The sensor is entirely fabricated using biodegradable materials, and the resonance frequency shift is based on the capacitance variation of its capacitor component (Figure 13c). First, the fringe-field capacitive sensor is wrapped around a polyolefin tube and then they integrate it in vivo arterial blood. Deng et al.[238] evaluated neovascularization and cellular proliferation by continuously monitoring the pressure of the wound site with an LC sensor embedded in a commercial bandage (Figure 12d). They tested the sensor embedded in the bandage both on pork skin and a foam. The sensor detected low pressure with a sensitivity of −270.8 kHz/mmHg and a linearity in the range of 0–200 mmHg. Moreover, other works were performed to improve the performance of wireless capacitive sensors in various applications, such as tactile sensing and human motion sensing, such as hand bending and facial muscle movements. For example, Nie et al.[254] improved the performance of an LC wireless sensor for tactile application by integrating a droplet-based capacitance-sensing unit with two circular planar coils. The passive sensor integrated on the fingertips was tested by monitoring the changes in the tactile force in table tennis. In addition, Kou et al.[255] improved the performance of the LC pressure sensor using a continuous wrinkled gold pattern for the inductor and the electrode of the capacitive part, whereas the dielectric layer was made of a micro-patterned Gr/PDMS composite. They wirelessly detected hand bending and facial muscle movements.

Monitoring of the damage and degradation in the structure is essential to enable early warnings about structural health. The wireless transmission systems for the health monitoring of large structures are mainly discussed in the last decades, especially for in situ health monitoring systems and some advanced industrial and engineering applications, such as torque sensing and point stress for ball bearings, blades, and rotating shafts. Various LC sensors have been developed to avoid catastrophic damage (in composite, steel, and concrete) through crack[249,256–259] and strain[254,255,260,261] sensing, thereby achieving reliable system monitoring, understanding material fatigue, and optimizing system performance. In 2005, Matsuzaki et al.[262] proposed a wireless strain sensor based on the oscillation circuit method to monitor car tires, where the steel wires were employed as electrodes to measure the changes in tire capacitance. The LC sensor presented in Figure 13e was developed for real-time pipeline integrity monitoring.[253] The sensor monitored the external corrosion of a metal pipe, where a water ingress or gas diffusion in the pipe affects the distance between the metal pipe and the coating lift-off from the pipeline, thus resulting in a capacitance variation of the interdigitated capacitor. These studies revealed that the LC wireless sensors with a free wire, free battery, small size, long interrogating distance, and several advantages, such as flexibility and ease of production and implementation, are very promising in real-time monitoring and data harvesting.

6. Conclusion

The present review highlights recent developments in capacitive strain sensors. The strain sensors based on electrical signal variation offer significant advantages, making them the most suitable method for various applications. Different studies have revealed that the capabilities of the capacitive strain sensors outperform those of resistive strain sensors. So far, resistive strain sensors are more commonly applied owing to their advantages, such as ease of use and the low sensitivity of capacitive strain sensors that use the geometric effect to induce capacitance variation. Researchers have successfully increased the gauge factor (GF) of capacitive strain sensors by changing the shape of the electrodes using new materials, such as ionic hydrogels, or focusing on the variation of the permittivity of the dielectric material. The soft capacitive sensor demonstrated high performance and the ability to measure strain over large structural areas or to detect local strain. Networks of independent capacitive sensors over the sensing region at the desired spatial resolution and a connected capacitive array of distributed mechanical sensors are the two leading technologies that can be used for detecting local deformation and area sensing. Recently, many new approaches based on the capacitive sensor have emerged for detecting local pressure, for example, by using a non-ideal flexible capacitor where the sensor is considered as a transmission line or by the electric field variation in an ionic gel layer. We also reviewed the capacitive interface circuits used for collecting data from the sensor and analyzing it before being received by the recipient. Several circuits have been reported to read out the capacitance difference, such as the CDC. The CDC sensing techniques that can be used for pure capacitive sensors are charge transfer, successive approximation, and sigma-delta modulation. Other sensing techniques have been developed for the capacitive sensor with high resistive electrodes, such as the gain and phase method, the cutoff frequency of a high-pass filter shift, the hyperplane approximation method, and the current integration methods. We also discussed the possibility of achieving remote sensing through the integration of the capacitive sensor on an oscillator circuit. The passive LC resonant sensors are the ideal systems for complex measurements in harsh environments owing to their ability to detect mechanical deformation without external power supplies or wired connections. These sensors can be easily realized by connecting the capacitive sensor with a spiral inductor in the same flexible substrate. The signal can be collected by electromagnetic coupling with an external readout coil. LC tags are highly preferred in many applications owing to their wireless detection capability.

Acknowledgements

The research reported in this publication was financially supported by King Abdullah University of Science and Technology (KAUST), Saudi Arabia, under the award number BAS/1/1315-01-01.

Conflict of Interest

The authors declare no conflict of interest.

Author Contributions

H.N. and G.L. conceptualized the study. All authors contributed to writing and editing the manuscript.

Keywords

capacitive variation mechanism, distributed strain, electronic interface, LC oscillator, strain sensor, wireless detection

Received: February 25, 2021
Revised: June 2, 2021
Published online:

[1] Y. Zheng, Z.-W. Zhu, W. Xiao, Q.-X. Deng, *Opt. Fiber Technol.* **2020**, *54*, 102127.
[2] Y. Zheng, Z.-W. Zhu, Q.-X. Deng, F. Xiao, *Opt. Fiber Technol.* **2019**, *49*, 28.
[3] G.-X. Fan, F.-T. Lin, P. Li, J.-G. Han, H.-S. Shang, Y. Wang, H. Zheng, *Sensors* **2020**, *20*, 2288.

[4] H. Tang, H. Ren, L. Jia, *IOP Conf. Ser.: Mater. Sci. Eng.* **2019**, *686*, 012027.
[5] J.-B. Chossat, Y.-L. Park, R. J. Wood, V. Duchaine, *IEEE Sens. J.* **2013**, *13*, 3405.
[6] J. Wan, Q. Wang, S. Zang, X. '. Huang, T. Wang, G. Liu, C. Li, X. Ren, *Compos. Sci. Technol.* **2019**, *182*, 107707.
[7] A. D. Kersey, T. A. Berkoff, W. W. Morey, *Electron. Lett.* **1992**, *28*, 236.
[8] W. Qiu, Y.-L. Kang, Z.-K. Lei, Q.-H. Qin, Q. Li, Q. Wang, *J. Raman Spectrosc.* **2010**, *41*, 1216.
[9] D. A. Henderson, R. W. Gordon, J. W. Hollkamp, G. S. Agnes, US5911158A, **1999**.
[10] J. Sirohi, I. Chopra, *J. Intell. Mater. Syst. Struct.* **2000**, *11*, 246,
[11] Alamusi, N. Hu, H. Fukunaga, S. Atobe, Y. Liu, J. Li, *Sensors* **2011**, *11*, 10691.
[12] J. Rantala, J. Hännikäinen, J. Vanhala, *Pers. Ubiquitous Comput.* **2011**, *15*, 85.
[13] M. Rosenberger, S. Hessler, S. Belle, B. Schmauss, R. Hellmann, *Opt. Express* **2014**, *22*, 5483.
[14] R. Rahimi, M. Ochoa, W. Yu, B. Ziaie, *ACS Appl. Mater. Interfaces* **2015**, *7*, 4463.
[15] S. Sony, S. Laventure, A. Sadhu, *Struct. Control Health Monit.* **2019**, *26*, e2321.
[16] L. E. Aygun, V. Kumar, C. Weaver, M. Gerber, S. Wagner, N. Verma, B. Glisic, J. C. Sturm, *Sensors* **2020**, *20*, 1386.
[17] X. Sun, Z. Qin, L. Ye, H. Zhang, Q. Yu, X. Wu, J. Li, F. Yao, *Chem. Eng. J.* **2020**, *382*, 122832.
[18] A. R. Burton, P. Sun, J. P. Lynch, *Struct. Health Monit.* **2019**, *20*, 749.
[19] Y. Lee, J. Kim, H. Joo, M. S. Raj, R. Ghaffari, D.-H. Kim, *Adv. Mater. Technol.* **2017**, *2*, 1700053.
[20] Y. J. Hong, H. Jeong, K. W. Cho, N. Lu, D. -. H. Kim, *Adv. Funct. Mater.* **2019**, *29*, 1808247.
[21] S. Choi, S. I. Han, D. Kim, T. Hyeon, D.-H. Kim, *Chem. Soc. Rev.* **2019**, *48*, 1566.
[22] S. Hong, S. Lee, D.-H. Kim, *Proc. IEEE* **2019**, *107*, 2185.
[23] M. Tompkins, in *Adjunct Proc. 2019 ACM Int. Jt. Conf. Pervasive Ubiquitous Comput. Proc. 2019 ACM Int. Symp. Wearable Comput.*, Association for Computing Machinery, New York, NY **2019**, pp. 1047–1049.
[24] J. Ko, S. Jee, J. H. Lee, S. H. Kim, *Sens. Actuators, A* **2018**, *274*, 50.
[25] D. Wang, D. Li, M. Zhao, Y. Xu, Q. Wei, *Appl. Surf. Sci.* **2018**, *454*, 218.
[26] T. N. Ly, S. Park, *J. Ind. Eng. Chem.* **2020**, *82*, 122.
[27] J. Ma, P. Wang, H. Chen, S. Bao, W. Chen, H. Lu, *ACS Appl. Mater. Interfaces* **2019**, *11*, 8527.
[28] X. Liu, C. Lu, X. Wu, X. Zhang, *J. Mater. Chem. A* **2017**, *5*, 9824.
[29] J. Lee, S. Kim, J. Lee, D. Yang, B. C. Park, S. Ryu, I. Park, *Nanoscale* **2014**, *6*, 11932.
[30] M. Asadnia, A. G. P. Kottapalli, J. M. Miao, M. S. Triantafyllou, in *2015 28th IEEE Int. Conf. Micro Electro Mech. Syst.*IEEE, New York **2015**, pp. 678–681.
[31] J. C. Yeo, H. K. Yap, W. Xi, Z. Wang, C.-H. Yeow, C. T. Lim, *Adv. Mater. Technol.* **2016**, *1*, 1600018.
[32] E. L. White, J. C. Case, R. K. Kramer, *Sens. Actuators, A* **2017**, *253*, 188.
[33] S. Din, W. Xu, L. K. Cheng, S. Dirven, *IEEE Sens. J.* **2017**, *17*, 5678.
[34] W. Dang, E. S. Hosseini, R. Dahiya, in 2018 IEEE SENSORS, IEEE, New York **2018**, pp. 1–4.
[35] X. Liao, W. Song, X. Zhang, H. Huang, Y. Wang, Y. Zheng, *J. Mater. Chem. C* **2018**, *6*, 12841.
[36] R. Herbert, J.-H. Kim, Y. Kim, H. Lee, W.-H. Yeo, *Materials* **2018**, *11*, 187.
[37] Y. Xin, J. Zhou, X. Xua, G. Lubineau, *Nanoscale* **2017**, *9*, 10897.
[38] K. Huang, H. Ning, N. Hu, F. Liu, X. Wu, S. Wang, Y. Liu, R. Zou, W. Yuan, Alamusi, L. Wu, *Compos. Sci. Technol.* **2020**, *192*, 108105.
[39] J. Gu, D. Kwon, J. Ahn, I. Park, *ACS Appl. Mater. Interfaces* **2020**, *12*, 10908.
[40] X. Fu, M. Ramos, A. M. Al-Jumaily, A. Meshkinzar, X. Huang, *J. Mater. Sci.* **2019**, *54*, 2170.
[41] J. T. Muth, D. M. Vogt, R. L. Truby, Y. Mengüç, D. B. Kolesky, R. J. Wood, J. A. Lewis, *Adv. Mater.* **2014**, *26*, 6307.
[42] A. Mehmood, N. M. Mubarak, M. Khalid, R. Walvekar, E. C. Abdullah, M. T. H. Siddiqui, H. A. Baloch, S. Nizamuddin, S. Mazari, *J. Environ. Chem. Eng.* **2020**, *8*, 103743.
[43] J. Zhao, G.-Y. Zhang, D.-X. Shi, *Chin. Phys. B* **2013**, *22*, 057701.
[44] S.-H. Bae, Y. Lee, B. K. Sharma, H.-J. Lee, J.-H. Kim, J.-H. Ahn, *Carbon* **2013**, *51*, 236.
[45] F. Xu, Y. Zhu, *Adv. Mater.* **2012**, *24*, 5117.
[46] M. Amjadi, A. Pichitpajongkit, S. Lee, S. Ryu, I. Park, *ACS Nano* **2014**, *8*, 5154.
[47] S. Zhang, H. Liu, S. Yang, X. Shi, D. Zhang, C. Shan, L. Mi, C. Liu, C. Shen, Z. Guo, *ACS Appl. Mater. Interfaces* **2019**, *11*, 10922.
[48] C. Farcau, N. M. Sangeetha, H. Moreira, B. Viallet, J. Grisolia, D. Ciuculescu-Pradines, L. Ressier, *ACS Nano* **2011**, *5*, 7137.
[49] S. Seyedin, J. M. Razal, P. C. Innis, A. Jeiranikhameneh, S. Beirne, G. G. Wallace, *ACS Appl. Mater. Interfaces* **2015**, *7*, 21150.
[50] D. Y. Choi, M. H. Kim, Y. S. Oh, S.-H. Jung, J. H. Jung, H. J. Sung, H. W. Lee, H. M. Lee, *ACS Appl. Mater. Interfaces* **2017**, *9*, 1770.
[51] C. Wang, X. Li, E. Gao, M. Jian, K. Xia, Q. Wang, Z. Xu, T. Ren, Y. Zhang, *Adv. Mater.* **2016**, *28*, 6640.
[52] N. Hu, Y. Karube, M. Arai, T. Watanabe, C. Yan, Y. Li, Y. Liu, H. Fukunaga, *Carbon* **2010**, *48*, 680.
[53] N. Hu, Y. Karube, C. Yan, Z. Masuda, H. Fukunaga, *Acta Mater.* **2008**, *56*, 2929.
[54] Y. Wang, R. Cao, C. Li, R. N. Dean, *IEEE Sens. J.* **2020**, *21*, 92.
[55] H. Sun, K. Dai, W. Zhai, Y. Zhou, J. Li, G. Zheng, B. Li, C. Liu, C. Shen, *ACS Appl. Mater. Interfaces* **2019**, *11*, 36052.
[56] Y. Lu, M. C. Biswas, Z. Guo, J.-W. Jeon, E. K. Wujcik, *Biosens. Bioelectron.* **2019**, *123*, 167.
[57] J. Shintake, E. Piskarev, S. H. Jeong, D. Floreano, *Adv. Mater. Tech.* **2018**, *3*, 1700284.
[58] M. Amjadi, K.-U. Kyung, I. Park, M. Sitti, *Adv. Funct. Mater.* **2016**, *26*, 1678.
[59] S. Yao, Y. Zhu, *Nanoscale* **2014**, *6*, 2345.
[60] C.-X. Liu, J.-W. Choi, *Microelectron. Eng.* **2014**, *117*, 1.
[61] L. Cai, L. Song, P. Luan, Q. Zhang, N. Zhang, Q. Gao, D. Zhao, X. Zhang, M. Tu, F. Yang, W. Zhou, Q. Fan, J. Luo, W. Zhou, P. M. Ajayan, S. Xie, *Sci. Rep.* **2013**, *3*, 3048.
[62] O. P. Thakur, A. K. Singh, in *2008 3rd Int. Conf. Sensing Tech.*, IEEE, New York **2008**, pp. 467–471.
[63] M. Rosenthal, N. Bonwit, C. Duncheon, J. Heim, in Electroact. Polym. Actuators Devices, IEEE, New York **2007**, *6524*, p. 65241F.
[64] D. J. Cohen, D. Mitra, K. Peterson, M. M. Maharbiz, *Nano Lett.* **2012**, *12*, 1821.
[65] R. Wang, W. Xu, W. Shen, X. Shi, J. Huang, W. Song, *Inorg. Chem. Front.* **2019**, *6*, 3119.
[66] G. Wu, S. Li, J. Hu, M. Dong, K. Dong, X. Hou, X. Xiao, *Pigm. Resin Technol.* **2020**, https://doi.org/10.1108/PRT-10-2019-0098.
[67] D. Wang, Y. Huang, W. Cai, M. Tian, P. Liu, Y. Zhang, *J. Appl. Polym. Sci.* **2014**, *131*, 40342.
[68] H. Mei, C. Zhang, R. Wang, J. Feng, T. Zhang, *Sens. Actuators, A* **2015**, *233*, 118.
[69] R. Shi, Z. Lou, S. Chen, G. Shen, *Sci. China Mater.* **2018**, *61*, 1587.
[70] S. C. B. Mannsfeld, B. C.-K. Tee, R. M. Stoltenberg, C. V. H.-H. Chen, S. Barman, B. V. O. Muir, A. N. Sokolov, C. Reese, Z. Bao, *Nat. Mater.* **2010**, *9*, 859.
[71] C. Mattmann, F. Clemens, G. Tröster, *Sensors* **2008**, *8*, 3719.

[72] K. L. Dorsey, in *2019 2nd IEEE Int. Conf. Soft Rob.*, IEEE, New York **2019**, pp. 378–383.
[73] M. Kisić, N. Blaž, L. Živanov, M. Damnjanović, in 2019 42nd Int. Spring Semin. Electron. Tech. (ISSE), IEEE, New York **2019**, pp. 1–5.
[74] S.-J. Woo, J.-H. Kong, D.-G. Kim, J.-M. Kim, *J. Mater. Chem. C* **2014**, *2*, 4415.
[75] M. Amjadi, Y. J. Yoon, I. Park, *Nanotechnology* **2015**, *26*, 375501.
[76] Y. Cheng, R. Wang, H. Zhai, J. Sun, *Nanoscale* **2017**, *9*, 3834.
[77] H. Shi, M. Al-Rubaiai, C. M. Holbrook, J. Miao, T. Pinto, C. Wang, X. Tan, *Adv. Funct. Mater.* **2019**, *29*, 1809116.
[78] M. Varga, C. Ladd, S. Ma, J. Holbery, G. Tröster, *Lab Chip* **2017**, *17*, 3272.
[79] L. Chen, X. Chen, Z. Zhang, T. Li, T. Zhao, X. Li, J. Zhang, *J. Sens.* **2019**, *2019*, 1418374.
[80] R. Ramalingame, A. Lakshmanan, F. Müller, U. Thomas, O. Kanoun, *J. Sens. Sens. Syst.* **2019**, *8*, 87.
[81] S. Rosset, H. R. Shea, *Appl. Phys. A* **2013**, *110*, 281.
[82] S. Zhao, J. Li, D. Cao, G. Zhang, J. Li, K. Li, Y. Yang, W. Wang, Y. Jin, R. Sun, C.-P. Wong, *ACS Appl. Mater. Interfaces* **2017**, *9*, 12147.
[83] T. Cheng, Y.-Z. Zhang, W.-Y. Lai, Y. Chen, W.-J. Zeng, W. Huang, *J. Mater. Chem. C* **2014**, *2*, 10369.
[84] J. Jeong, S. Kim, J. Cho, Y. Hong, *IEEE Electron Device Lett.* **2009**, *30*, 1284.
[85] J. Xu, J. Chen, M. Zhang, J.-D. Hong, G. Shi, *Adv. Electron. Mater.* **2016**, *2*, 1600022.
[86] C. Jiang, Q. Li, S. Fan, Q. Guo, S. Bi, X. Wang, X. Cao, Y. Liu, J. Song, *Nano Energy* **2020**, *73*, 104782.
[87] F. Xu, W. Lu, Y. Zhu, *ACS Nano* **2011**, *5*, 672.
[88] C.-J. Lee, J. Park, C. Piao, H.-E. Seo, J. Choi, J.-H. Chun, *Sensors* **2018**, *18*, 3637.
[89] D. H. Ho, Q. Sun, S. Y. Kim, J. T. Han, D. H. Kim, J. H. Cho, *Adv. Mater.* **2016**, *28*, 2601.
[90] M. K. Filippidou, E. Tegou, V. Tsouti, S. Chatzandroulis, *Microelectron. Eng.* **2015**, *142*, 7.
[91] C. G. Ma, D. Y. Xi, M. Liu, *J. Compos. Mater.* **2013**, *47*, 1153.
[92] J. Wang, J. Jiu, T. Araki, M. Nogi, T. Sugahara, S. Nagao, H. Koga, P. He, K. Suganuma, *Nano-Micro Lett.* **2015**, *7*, 51.
[93] M. Segev-Bar, H. Haick, *ACS Nano* **2013**, *7*, 8366.
[94] S. Hwang, S.-H. Jeong, *Korean J. Chem. Eng.* **2016**, *33*, 2771.
[95] T. Yamada, Y. Hayamizu, Y. Yamamoto, Y. Yomogida, A. Izadi-Najafabadi, D. N. Futaba, K. Hata, *Nat. Nanotechnol.* **2011**, *6*, 296.
[96] G. Yun, S.-Y. Tang, H. Lu, S. Zhang, M. D. Dickey, W. Li, *Small Science* **2021**, *1*, 2000080.
[97] S. Yao, L. Vargas, X. Hu, Y. Zhu, *IEEE Sens. J.* **2018**, *18*, 3010.
[98] O. Atalay, A. Atalay, J. Gafford, H. Wang, R. Wood, C. Walsh, *Adv. Mater. Technol.* **2017**, *2*, 1700081.
[99] A. Atalay, V. Sanchez, O. Atalay, D. M. Vogt, F. Haufe, R. J. Wood, C. J. Walsh, *Adv. Mater. Technol.* **2017**, *2*, 1700136.
[100] A. Frutiger, J. T. Muth, D. M. Vogt, Y. Mengüç, A. Campo, A. D. Valentine, C. J. Walsh, J. A. Lewis, *Adv. Mater.* **2015**, *27*, 2440.
[101] J. Shintake, E. Piskarev, S. H. Jeong, D. Floreano, *Adv. Mater. Technol.* **2018**, *3*, 1700284.
[102] E. L. White, M. C. Yuen, J. C. Case, R. K. Kramer, *Adv. Mater. Technol.* **2017**, *2*, 1700072.
[103] U.-H. Shin, D.-W. Jeong, S.-M. Park, S.-H. Kim, H. W. Lee, J.-M. Kim, *Carbon* **2014**, *80*, 396.
[104] D. J. Lipomi, M. Vosgueritchian, B. C-K. Tee, S. L. Hellstrom, J. A. Lee, C. H. Fox, Z. Bao, *Nat. Nanotech.* **2011**, *6*, 788.
[105] J. Zhang, L. Wan, Y. Gao, X. Fang, T. Lu, L. Pan, F. Xuan, *Adv. Electron. Mater.* **2019**, *5*, 1900285.
[106] C. Deng, L. Lan, P. He, C. Ding, B. Chen, W. Zheng, X. Zhao, W. Chen, X. Zhong, M. Li, H. Tao, J. Peng, Y. Cao, *J. Mater. Chem. C* **2020**, *8*, 5541.
[107] S.-R. Kim, J.-H. Kim, J.-W. Park, *ACS Appl. Mater. Interfaces* **2017**, *9*, 26407.
[108] J. Shintake, T. Nagai, K. Ogishima, *Front. Robot. AI* **2019**, *6*, 127.
[109] R. Nur, N. Matsuhisa, Z. Jiang, M. O. G. Nayeem, T. Yokota, T. Someya, *Nano Lett.* **2018**, *18*, 5610.
[110] H. Nesser, J. Grisolia, T. Alnasser, B. Viallet, L. Ressier, *Nanoscale* **2018**, *10*, 10479.
[111] J. Yuan, A. Luna, W. Neri, C. Zakri, A. Colin, P. Poulin, *ACS Nano* **2018**, *12*, 1688.
[112] H. Nesser, G. Lubineau, *ACS Mater. Interfaces* **2021**, https://doi.org/10.1021/acsami.1c07704.
[113] H. Xu, Y. Lv, D. Qiu, Y. Zhou, H. Zeng, Y. Chu, *Nanoscale* **2019**, *11*, 1570.
[114] J. Yuan, *Chin. Chem. Lett.* **2017**, *28*, 2036.
[115] B. Nie, R. Li, J. Cao, J. D. Brandt, T. Pan, *Adv. Mater.* **2015**, *27*, 6055.
[116] H. Ota, K. Chen, Y. Lin, D. Kiriya, H. Shiraki, Z. Yu, T.-J. Ha, A. Javey, *Nat. Commun.* **2014**, *5*, 5032.
[117] J.-Y. Sun, C. Keplinger, G. M. Whitesides, Z. Suo, *Adv. Mater.* **2014**, *26*, 7608.
[118] C. Keplinger, J.-Y. Sun, C. C. Foo, P. Rothemund, G. M. Whitesides, Z. Suo, *Science* **2013**, *341*, 984.
[119] J. H. Cho, J. Lee, Y. Xia, B. Kim, Y. He, M. J. Renn, T. P. Lodge, C. Daniel Frisbie, *Nat. Mater.* **2008**, *7*, 900.
[120] V. Narasimhan, S.-Y. Park, *Langmuir* **2015**, *31*, 8512.
[121] H. Du, X. Lin, Z. Xu, D. Chu, *J. Mater. Sci.* **2015**, *50*, 5641.
[122] X. Li, R. Zhang, W. Yu, K. Wang, J. Wei, D. Wu, A. Cao, Z. Li, Y. Cheng, Q. Zheng, R. S. Ruoff, H. Zhu, *Sci. Rep.* **2012**, *2*, 870.
[123] S. Li, G. Liu, L. Wang, G. Fang, Y. Su, *Adv. Electron. Mater.* **2020**, *6*, 2000618.
[124] Y. Yao, B. Glisic, *Sensors* **2015**, *15*, 8088.
[125] T. Someya, T. Sekitani, S. Iba, Y. Kato, H. Kawaguchi, T. Sakurai, *Proc. Natl. Acad. Sci. USA* **2004**, *101*, 9966.
[126] K. Takei, T. Takahashi, J. C. Ho, H. Ko, A. G. Gillies, P. W. Leu, R. S. Fearing, A. Javey, *Nat. Mater.* **2010**, *9*, 821.
[127] K. J. Loh, J. Kim, J. P. Lynch, N. W. S. Kam, N. A. Kotov, *Smart Mater. Struct.* **2007**, *16*, 429.
[128] L. Pan, A. Chortos, G. Yu, Y. Wang, S. Isaacson, R. Allen, Y. Shi, R. Dauskardt, Z. Bao, *Nat. Commun.* **2014**, *5*, 3002.
[129] H.-B. Yao, J. Ge, C.-F. Wang, X. Wang, W. Hu, Z.-J. Zheng, Y. Ni, S.-H. Yu, *Adv. Mater.* **2013**, *25*, 6692.
[130] Y. Zhang, G. Laput, C. Harrison, in *Proc. 2017 CHI Conf. Hum. Factors Comput. Syst.*, Denver, CO **2017**, pp. 1–14.
[131] X. Yi, C. Cho, J. Cooper, Y. Wang, M. M. Tentzeris, R. T. Leon, *Smart Mater. Struct.* **2013**, *22*, 085009.
[132] I. Mohammad, H. Huang, *Smart Mater. Struct.* **2010**, *19*, 055023.
[133] S. Laflamme, F. Ubertini, H. Saleem, A. D'alessandro, A. Downey, H. Ceylan, A. L. Materazzi, *J. Struct. Eng.* **2015**, *141*, 04014186.
[134] S. Laflamme, M. Kollosche, J. J. Connor, G. Kofod, *J. Eng. Mech.* **2013**, *139*, 879.
[135] X. Kong, J. Li, W. Collins, C. Bennett, S. Laflamme, H. Jo, *Smart Mater. Struct.* **2017**, *26*, 085024.
[136] R. K. Kramer, C. Majidi, R. J. Wood, in *2011 IEEE Int. Conf. Rob. Autom.*, IEEE, New York **2011**, pp. 1103–1107.
[137] A. P. Gerratt, H. O. Michaud, S. P. Lacour, *Adv. Funct. Mater.* **2015**, *25*, 2287.
[138] N. Farrow, L. McIntire, N. Correll, in *2017 IEEE Int. Conf. Rob. Autom.*, IEEE, New York **2017**, pp. 5525–5531.
[139] M. Acer, M. Salerno, K. Agbeviade, J. Paik, *Smart Mater. Struct.* **2015**, *24*, 075030.
[140] M.-Y. Cheng, C.-M. Tsao, Y.-Z. Lai, Y.-J. Yang, *Sens. Actuators, A* **2011**, *166*, 226.
[141] B.-Y. Lee, J. Kim, H. Kim, C. Kim, S.-D. Lee, *Sens. Actuators, A* **2016**, *240*, 103.
[142] H. Vandeparre, D. Watson, S. P. Lacour, *Appl. Phys. Lett.* **2013**, *103*, 204103.

[143] C. Larson, J. Spjut, R. Knepper, R. Shepherd, *Soft Rob.* **2019**, *6*, 611.
[144] J. Lee, H. Kwon, J. Seo, S. Shin, J. H. Koo, C. Pang, S. Son, J. H. Kim, Y. H. Jang, D. E. Kim, T. Lee, *Adv. Mater.* **2015**, *27*, 2433.
[145] D. J. Lipomi, M. Vosgueritchian, B. C.-K. Tee, S. L. Hellstrom, J. A. Lee, C. H. Fox, Z. Bao, *Nat. Nanotechnol.* **2011**, *6*, 788.
[146] G. Walker, *J. Soc. Inf. Disp.* **2012**, *20*, 413.
[147] I.-S. Yang, O.-K. Kwon, *IEEE Trans. Consum. Electron.* **2011**, *57*, 1027.
[148] G. Walker, *Touch Apple iPhone* **2007**, *5*, 5.
[149] R. Matsuda, S. Mizuguchi, F. Nakamura, T. Endo, G. Inamori, Y. Isoda, H. Ota, in *2020 IEEE 33rd Int. Conf. Micro Electro Mech. Syst. (MEMS)*, IEEE, New York **2020**, pp. 803–805.
[150] Y.-L. Park, C. Majidi, R. Kramer, P. Bérard, R. J. Wood, *J. Micromech. Microeng.* **2010**, *20*, 125029.
[151] B. Li, Y. Gao, A. Fontecchio, Y. Visell, *Smart Mater. Struct.* **2016**, *25*, 075009.
[152] M. S. Sarwar, Y. Dobashi, C. Preston, J. K. M. Wyss, S. Mirabbasi, J. D. W. Madden, *Sci. Adv.* **2017**, *3*, e1602200.
[153] H.-K. Kim, S. Lee, K.-S. Yun, *Sens. Actuators, A* **2011**, *165*, 2.
[154] W. Hu, X. Niu, R. Zhao, Q. Pei, *Appl. Phys. Lett.* **2013**, *102*, 083303.
[155] K. Kim, G. Song, C. Park, K.-S. Yun, *Sensors* **2017**, *17*, 2582.
[156] Y. Zhu, S. Rosset, I. A. Anderson, *Electroact. Polym. Actuators Devices*, IEEE, New York **2018**, *10594*, p. 105942J.
[157] A. Meyer, S. Lenz, S. Gratz-Kelly, P. Motzki, S. Nalbach, S. Seelecke, G. Rizzello, in *Electroact. Polym. Actuators Devices*, IEEE, New York **2020**, *11375*, p. 1137528.
[158] H.-K. Lee, S.-I. Chang, E. Yoon, *J. Microelectromech. Syst.* **2006**, *15*, 1681.
[159] A. Downey, S. Laflamme, F. Ubertini, *Smart Mater. Struct.* **2017**, *26*, 125005.
[160] H. Saleem, A. Downey, S. Laflamme, M. Kollosche, F. Ubertini, *Mater. Eval.* **2015**, *73*, 1384.
[161] A. Downey, S. Laflamme, F. Ubertini, *Meas. Sci. Technol.* **2016**, *27*, 124016.
[162] X. Kong, J. Li, W. Collins, C. Bennett, S. Laflamme, H. Jo, *Smart Mater. Struct.* **2018**, *27*, 115008.
[163] A. Downey, A. D'Alessandro, F. Ubertini, S. Laflamme, Sens. Smart Struct. Tech. Civil, Mech. Aerosp. Syst. 2018, SPIE, Bellingham, WA **2018**, *10598*, p. 105983B.
[164] M. Kang, J. Kim, B. Jang, Y. Chae, J.-H. Kim, J.-H. Ahn, *ACS Nano* **2017**, *11*, 7950.
[165] Q. Hua, J. Sun, H. Liu, R. Bao, R. Yu, J. Zhai, C. Pan, Z. L. Wang, *Nat. Commun.* **2018**, *9*, 244.
[166] O. Glauser, S. Wu, D. Panozzo, O. Hilliges, O. Sorkine-Hornung, *ACM Trans. Graphics* **2019**, *38*, 41.
[167] O. Glauser, D. Panozzo, O. Hilliges, O. Sorkine-Hornung, *ACM Trans. Graphics* **2019**, *38*, 16.
[168] X. Kong, J. Li, C. Collins, C. Bennett, H. Jo, J. H. Jeong, S. Laflamme, *Sens. Smart Struct. Tech. Civil, Mech. Aerosp. Syst.* 2018, SPIE, Bellingham, WA **2018**, *10598*, p. 105980Q.
[169] S. Walia, I. Mondal, G. U. Kulkarni, *ACS Appl. Electron. Mater.* **2019**, *1*, 1597.
[170] Y. Xia, Q. Zhang, X. E. Wu, T. V. Kirk, X. D. Chen, *Sensors* **2019**, *19*, 4553.
[171] B. J. Park, S. Oh, F. S. Kim, S. T. Chang, *J. Mater. Chem. C* **2019**, *7*, 10264.
[172] C.-C. Kim, H.-H. Lee, K. H. Oh, J.-Y. Sun, *Science* **2016**, *353*, 682.
[173] H. Wang, Q. Tang, X. Zhao, Y. Tong, Y. Liu, *ACS Appl. Mater. Interfaces* **2018**, *10*, 2785.
[174] S. G. Yoon, S. T. Chang, *J. Mater. Chem. C* **2017**, *5*, 1910.
[175] H. A. Sonar, M. C. Yuen, R. Kramer-Bottiglio, J. Paik, in *2018 IEEE Int. Conf. Soft Rob.*, IEEE, New York **2018**, pp. 170–175.
[176] D. Xu, A. Tairych, I. A. Anderson, *Smart Mater. Struct.* **2015**, *25*, 015012.
[177] D. Xu, A. Tairych, I. A. Anderson, *J. Polym. Sci., Part B: Polym. Phys.* **2016**, *54*, 465.
[178] E. L. White, M. C. Yuen, R. K. Kramer, in 2017 IEEE SENSORS, IEEE, New York **2017**, pp. 1–3.
[179] V. P. Petkov, B. E. Boser, *IEEE J. Solid-State Circuits* **2005**, *40*, 1602.
[180] W. Bracke, P. Merken, R. Puers, C. Van Hoof, *IEEE Trans. Circuits Syst.* **2007**, *54*, 130.
[181] S. Pavan, R. Schreier, G. C. Temes, *Understanding Delta-Sigma Data Converters*, John Wiley & Sons, New York **2017**.
[182] H. Omran, A. Alhoshany, H. Alahmadi, K. N. Salama, in *2016 IEEE Symp. VLSI Circuits (VLSI-Circuits)*, IEEE, New York **2016**, pp. 1–2.
[183] H. Ha, D. Sylvester, D. Blaauw, J.-Y. Sim, in *2014 IEEE Int. Solid-State Circuits Conf. Dig. Tech. Pap.*, IEEE, New York **2014**, pp. 220–221.
[184] H. Omran, M. Arsalan, K. N. Salama, in *Proc. IEEE 2014 Custom Integr. Circuits Conf.*, IEEE, New York **2014**, pp. 1–4.
[185] L. Zhong, X. Lai, D. Xu, *IEEE J. Solid-State Circuits* **2018**, *53*, 2240.
[186] J. O'Dowd, A. Callanan, G. Banarie, E. Company-Bosch, in 2005 IEEE SENSORS **2005**, 4.
[187] F. Reverter, M. Gasulla, R. Pallas-Areny, in *Proc. 21st IEEE Instrum. Meas. Technol. Conf.* **2004**, *3*, pp. 1771-1775.
[188] J. E. Gaitan-Pitre, M. Gasulla, R. Pallas-Areny, in 2007 IEEE Instrum. Meas. Technol. Conf. IMTC 2007, IEEE, New York **2007**, pp. 1–5.
[189] P. H. Dietz, D. Leigh, W. S. Yerazunis, *2002 IEEE SENSORS* **2002**, *1*, 715.
[190] J. Meyer, B. Arnrich, J. Schumm, G. Troster, *IEEE Sens. J.* **2010**, *10*, 1391.
[191] D. S. Kim, N. H. Chuc, S. M. Jin, K. J. An, V. H. Phuc, J. Koo, R. R. Choi, in *Electroact. Polym. Actuators Devices*, IEEE, New York **2010**, *7642*, p. 76420F.
[192] B. C. Kim, S. Shin, J. Chung, Y. Lee, J. D. Nam, H. Moon, J. C. Koo, in *Electroact. Polym. Actuators Devices*, IEEE, New York **2011**, *7976*, p. 797628.
[193] D. Kim, C. H. Lee, B. C. Kim, D. H. Lee, H. S. Lee, C. T. Nguyen, H. R. Choi, in *Electroact. Polym. Actuators Devices*, IEEE, New York **2013**, *8687*, p. 86872J.
[194] D. P. J. Cotton, I. M. Graz, S. P. Lacour, *IEEE Sens. J.* **2009**, *9*, 2008.
[195] A. P. Gerratt, N. Sommer, S. P. Lacour, A. Billard, in *2014 IEEE-RAS Int. Conf. Humanoid Rob.*, IEEE, New York **2014**, pp. 238–245.
[196] Z. Cui, F. R. Poblete, G. Cheng, S. Yao, X. Jiang, Y. Zhu, *J. Mater. Res.* **2015**, *30*, 79.
[197] Y. Iskandarani, H. R. Karimi, *IEEE Sens. J.* **2012**, *12*, 2616.
[198] X. Ma, J. Guo, K.-M. Lee, L. Yang, M. Chen, in *Intelligent Robotics and Applications*, Springer, Cham **2019**,467–479.
[199] X. Guo, Y. Huang, X. Cai, C. Liu, P. Liu, *Meas. Sci. Technol.* **2016**, *27*, 045105.
[200] StretchSense: Premium hand motion capture solution, Electronics manufacturer in Auckland, New Zealand, https://stretchsense.com.
[201] Y. Yang, K. Xu, T. Vervust, J. Vanfleteren, *Sens. Actuators, B* **2018**, *261*, 144.
[202] P. Lotz, M. Matysek, K. Flittner, H. F. Schlaak, in *Electroact. Polym. Actuators Devices*, IEEE, New York **2010**, *7642*, p. 764214.
[203] J. Maas, M. Griese, T. Hoffstadt, "Integrated Sensor Concepts for Dielectric Elastomer Actuators." *Proceedings of the ASME 2013 Conference on Smart Materials, Adaptive Structures and Intelligent Systems. Volume 2: Mechanics and Behavior of Active Materials; Structural Health Monitoring; Bioinspired Smart Materials and Systems; Energy Harvesting*, Snowbird, Utah, USA. September 16–18 **2013**, V002T02A019. ASME. https://doi.org/10.1115/SMASIS2013-3243.
[204] T. Hoffstadt, M. Griese, J. Maas, *Smart Mater. Struct.* **2014**, *23*, 104007.

[205] G. Buchberger, B. Mayrhofer, B. Jakoby, W. Hilber, S. Bauer, in *2012 IEEE Int. Instrum. Meas. Tech. Conf. Proc.*, IEEE, New York **2012**, pp. 75–80.
[206] C. Keplinger, M. Kaltenbrunner, N. Arnold, S. Bauer, *Appl. Phys. Lett.* **2008**, *92*, 192903.
[207] J. A. Dobrzynska, M. A. M. Gijs, *J. Micromech. Microeng.* **2012**, *23*, 015009.
[208] G. Rizzello, D. Naso, A. York, S. Seelecke, in *2015 IEEE Int. Conf. Mechatron.*, IEEE, New York **2015**, pp. 300–306.
[209] K. Jung, K. J. Kim, H. R. Choi, *Sens. Actuators, A* **2008**, *143*, 343.
[210] A. York, J. Dunn, S. Seelecke, *Smart Mater. Struct.* **2013**, *22*, 094015.
[211] H. Haus, M. Matysek, H. Mößinger, H. F. Schlaak, *Smart Mater. Struct.* **2013**, *22*, 104009.
[212] T. A. Gisby, B. M. O'brien, I. A. Anderson, *Appl. Phys. Lett.* **2013**, *102*, 193703.
[213] M. Matysek, H. Haus, H. Moessinger, D. Brokken, P. Lotz, H. F. Schlaak, in *Electroact. Polym. Actuators Devices*, IEEE, New York **2011**, *7976*, 797612.
[214] H. Haus, M. Matysek, H. Moessinger, K. Flittner, H. F. Schlaak, in *Electroact. Polym. Actuators Devices*, IEEE, New York **2013**, *8687*, p. 86871D.
[215] I. Mohammad, V. Gowda, H. Zhai, H. Huang, *Meas. Sci. Technol.* **2011**, *23*, 015102.
[216] D. Xu, T. A. Gisby, S. Xie, I. A. Anderson, in *Electroact. Polym. Actuators Devices*, IEEE, New York **2013**, *8687*, p. 86872L.
[217] D. Xu, T. G. McKay, S. Michel, I. A. Anderson, in *Electroact. Polym. Actuators Devices*, IEEE, New York **2014**, *9056*, p. 90561A.
[218] J. Xiong, Y. Li, Y. Hong, B. Zhang, T. Cui, Q. Tan, S. Zheng, T. Liang, *Sens. Actuators, A* **2013**, *197*, 30.
[219] J. A. Henao-Sepulveda, M. Toledo-Quinones, Y. Jia, in 2005 IEEE Int. Instrum. Meas. Tech. Conf. Proc., IEEE, New York **2005**, *2*, p. 1571.
[220] S. Scott, A. Kovacs, L. Gupta, J. Katz, F. Sadeghi, D. Peroulis, in *2011 IEEE 24th Int. Conf. Micro Electro Mech. Syst.*, IEEE, New York **2011**, pp. 660–663.
[221] X. Xu, H. Huang, *Smart Mater. Struct.* **2011**, *21*, 015004.
[222] M. H. M. Kouhani, J. Wu, A. Tavakoli, A. J. Weber, W. Li, *Lab Chip* **2020**, *20*, 332.
[223] W.-J. Deng, L.-F. Wang, L. Dong, Q.-A. Huang, *IEEE Sens. J.* **2018**, *18*, 4886.
[224] W. Gao, S. Emaminejad, H. Y. Y. Nyein, S. Challa, K. Chen, A. Peck, H. M. Fahad, H. Ota, H. Shiraki, D. Kiriya, D.-H. Lien, G. A. Brooks, R. W. Davis, A. Javey, *Nature* **2016**, *529*, 509.
[225] S. Han, J. Kim, S. M. Won, Y. Ma, D. Kang, Z. Xie, K.-T. Lee, H. U. Chung, A. Banks, S. Min, S. Y. Heo, C. R. Davies, J. W. Lee, C.-H. Lee, B. H. Kim, K. Li, Y. Zhou, C. Wei, X. Feng, Y. Huang, J. A. Rogers, *Sci. Transl. Med.* **2018**, *10*, eaan4950.
[226] A. J. Bandodkar, P. Gutruf, J. Choi, K. Lee, Y. Sekine, J. T. Reeder, W. J. Jeang, A. J. Aranyosi, S. P. Lee, J. B. Model, R. Ghaffari, C.-J. Su, J. P. Leshock, T. Ray, A. Verrillo, K. Thomas, V. Krishnamurthi, S. Han, J. Kim, S. Krishnan, T. Hang, J. A. Rogers, *Sci. Adv.* **2019**, *5*, eaav3294.
[227] J. Kim, A. Banks, H. Cheng, Z. Xie, S. Xu, K.-I. Jang, J. W. Lee, Z. Liu, P. Gutruf, X. Huang, P. Wei, F. Liu, K. Li, M. Dalal, R. Ghaffari, X. Feng, Y. Huang, S. Gupta, U. Paik, J. A. Rogers, *Small* **2015**, *11*, 906.
[228] S. Niu, N. Matsuhisa, L. Beker, J. Li, S. Wang, J. Wang, Y. Jiang, X. Yan, Y. Yun, W. Burnett, A. S. Y. Poon, J. B.-H. Tok, X. Chen, Z. Bao, *Nat. Electron.* **2019**, *2*, 361.
[229] H. Kou, L. Zhang, Q. Tan, G. Liu, H. Dong, W. Zhang, J. Xiong, *Sci. Rep.* **2019**, *9*, 3916.
[230] R. Nopper, R. Niekrawietz, L. Reindl, *IEEE Trans. Instrum. Meas.* **2010**, *59*, 2450.
[231] Q.-A. Huang, L. Dong, L.-F. Wang, *J. Microelectromech. Syst.* **2016**, *25*, 822.
[232] C. C. Collins, *IEEE Trans. Biomed. Eng.* **1967**, *BME-14*, 74.
[233] B. Nie, R. Huang, T. Yao, Y. Zhang, Y. Miao, C. Liu, J. Liu, X. Chen, *Adv. Funct. Mater.* **2019**, *29*, 1808786.
[234] J. Zhu, J. J. Fox, N. Yi, H. Cheng, *ACS Appl. Mater. Interfaces* **2019**, *11*, 8867.
[235] L. Song, A. C. Myers, J. J. Adams, Y. Zhu, *ACS Appl. Mater. Interfaces* **2014**, *6*, 4248.
[236] Y. Tai, Z. Yang, *Adv. Mater. Interfaces* **2017**, *4*, 1700496.
[237] H. Kou, L. Zhang, Q. Tan, G. Liu, W. Lv, F. Lu, H. Dong, J. Xiong, *Sens. Actuators, A* **2018**, *277*, 150.
[238] J. Salmerón, A. Albrecht, S. Kaffah, M. Becherer, P. Lugli, A. Rivadeneyra, *Sensors* **2018**, *18*, 2275.
[239] M. Nabipoor, B. Y. Majlis, *J. Phys.: Conf. Ser.* **2006**, *34*, 770.
[240] H. Kairm, D. Delfin, M. A. I. Shuvo, L. A. Chavez, C. R. Garcia, J. H. Barton, S. M. Gaytan, M. A. Cadena, R. C. Rumpf, R. B. Wicker, Y. Lin, A. Choudhuri, *IEEE Sens. J.* **2015**, *15*, 1445.
[241] Q. Tan, W. Lv, Y. Ji, R. Song, F. Lu, H. Dong, W. Zhang, J. Xiong, *Sens. Actuators, B* **2018**, *270*, 433.
[242] M.-Z. Xie, L.-F. Wang, L. Dong, W.-J. Deng, Q.-A. Huang, *IEEE Sens. J.* **2019**, *19*, 4717.
[243] J. C. Butler, A. J. Vigliotti, F. W. Verdi, S. M. Walsh, *Sens. Actuators, A* **2002**, *102*, 61.
[244] B. Ozbey, V. Erturk, H. Demir, A. Altintas, O. Kurc, *Sensors* **2016**, *16*, 496.
[245] M. F. Kuhn, G. P. Breier, A. R. P. Dias, T. G. R. Clarke, *J. Nondestr. Eval.* **2018**, *37*, 22.
[246] Y. Jia, K. Sun, F. J. Agosto, M. T. Quiñones, *Meas. Sci. Technol.* **2006**, *17*, 2869.
[247] X. Huang, Y. Liu, K. Chen, W.-J. Shin, C.-J. Lu, G.-W. Kong, D. Patnaik, S.-H. Lee, J. F. Cortes, J. A. Rogers, *Small* **2014**, *10*, 3083.
[248] W.-J. Deng, L. I.-F. Wang, L. Dong, Q.-A. N. Huang, *J. Microelectromech. Syst.* **2019**, *28*, 344.
[249] H. Kou, Q. Tan, Y. Wang, G. Zhang, S. Su, J. Xiong, *Sens. Actuators, B* **2020**, *311*, 127907.
[250] P.-J. Chen, S. Saati, R. Varma, M. S. Humayun, Y.-C. Tai, *J. Microelectromech. Syst.* **2010**, *19*, 721.
[251] F. Stauffer, Q. Zhang, K. Tybrandt, B. Llerena Zambrano, J. Hengsteler, A. Stoll, C. Trüeb, M. Hagander, J.-M. Sujata, F. Hoffmann, J. Schuurmans Stekhoven, J. Quack, H. Zilly, J. Goedejohann, M. P. Schneider, T. M. Kessler, W. R. Taylor, R. Küng, J. Vörös, *Adv. Mater. Technol.* **2018**, *3*, 1800031.
[252] C. M. Boutry, L. Beker, Y. Kaizawa, C. Vassos, H. Tran, A. C. Hinckley, R. Pfattner, S. Niu, J. Li, J. Claverie, Z. Wang, J. Chang, P. M. Fox, Z. Bao, *Nat. Biomed. Eng.* **2019**, *3*, 47.
[253] M. H. Zarifi, S. Deif, M. Daneshmand, *Sens. Actuators, A* **2017**, *261*, 24.
[254] J. Kim, Z. Wang, W. S. Kim, *IEEE Sens. J.* **2014**, *14*, 4395.
[255] J. Chuang, D. J. Thomson, G. E. Bridges, *Rev. Sci. Instrum.* **2005**, *76*, 094703.
[256] L. Ke, Z. Liu, H. Yu, *Sensors* **2019**, *19*, 110.
[257] J. Zhang, H. Huang, C. Huang, B. Zhang, Y. Li, K. Wang, D. Su, G. Y. Tian, *IEEE Trans. Antennas Propag.* **2019**, *67*, 5746.
[258] S. Xue, K. Xu, L. Xie, G. Wan, *Smart Mater. Struct.* **2019**, *28*, 085012.
[259] Z. Liu, H. Yu, K. Zhou, R. Li, *Proceedings* **2019**, *42*, 3.
[260] X. Yi, T. Wu, Y. Wang, M. M. Tentzeris, *IEEE Sens. J.* **2015**, *15*, 6147.
[261] O. O. Rakibet, C. V. Rumens, J. C. Batchelor, S. J. Holder, *IEEE Antennas Wireless Propag. Lett.* **2014**, *13*, 814.
[262] R. Matsuzaki, A. Todoroki, *Smart Mater. Struct.* **2005**, *14*, 561.
[263] B. Nie, T. Yao, Y. Zhang, J. Liu, X. Chen, *Appl. Phys. Lett.* **2018**, *112*, 031904.

Hussein Nesser received his B.S. (2010) and M.S. (2012) degrees in Condensed Material and Radiation from Joseph Fourier University, and subsequently obtained a Ph.D. degree in Materials Science and Electronics from the University of Bordeaux, France, in 2016. He worked as a Postdoctoral Fellow between 2017 and 2019 at INSA Toulouse, France. He is currently a Postdoctoral Fellow in KAUST in Saudi Arabia. His research interests mainly focus on the electromechanical characterization of functional nanocomposites for applications that include actuators, sensors, and energy harvesters.

Gilles Lubineau is Professor of Mechanical Engineering and Associate Dean at KAUST. Following his "aggregation" in theoretical mechanics, Prof. Lubineau earned a PhD degree in Mechanical Engineering and an habilitation for research from École Normale Supérieure de Cachan (ENS-Cachan). His current research interests include: integrity at short and/or long-term of composite materials and structures, inverse problems for constitutive parameters, multi-scale coupling technique, nano and multifunctional materials and devices.

